Article

Not peer-reviewed version

Methodology for the Analysis of Drought in Subtropical Crops with Remote Sensing and Predictive Models: Application in the Semi-Arid Region Southern Spain

David Carruana-Herrera *, Federico B. Galacho-Jiménez, José D. Ruiz-Sinoga

Posted Date: 15 September 2025

doi: 10.20944/preprints202509.1149.v1

Keywords: drought; remote sensing; imagery; subtropical crops; vegetation index

 doi:10.20944/preprints202509.1149.v1

Article

Methodology for the Analysis of Drought in Subtropical Crops with Remote Sensing and Predictive Models: Application in the Semi-Arid Region Southern Spain

David Carruana-Herrera [1,*], Federico B. Galacho-Jiménez [2] and José D. Ruiz-Sinoga [3]

[1] Geographic Analysis Research Group, Department of Geography, Teatinos Campus, University of Malaga, Malaga, 29010, Spain and Geomorphology and Soils Laboratory, Ada Byron Research Building, University of Malaga, Malaga, 29010, Spain

[2] Geographic Analysis Research Group, Department of Geography, Teatinos Campus, University of Malaga, Malaga, 29010, Spain

[3] Department of Geography, Teatinos Campus, University of Malaga, Malaga, 29010, Spain and Geomorphology and Soils Laboratory, Ada Byron Research Building, University of Malaga, Malaga, 29010, Spain

* Correspondence: carruana@uma.es

Abstract

This paper proposes a methodology based on the combined application of climate indices for precipitation and temperature along with multispectral Sentinel 2 imagery, used to generate vegetation indices that serve to diagnose the condition of subtropical irrigated crops through a predictive model. These crops demand significant irrigation, and in Mediterranean semi-arid environments, where water scarcity and drought periods are increasingly frequent and severe, this presents a serious problem. The aim of this methodological proposal is to address the need to adjust cultivated areas to actual water availability. It is now evident and necessary to implement efficient management of agricultural practices, avoiding the expansion of irrigated areas when there is not enough water available. As a result of this work, the climatic interrelation with the real condition of the crops is demonstrated.

Keywords: drought; remote sensing; imagery; subtropical crops; vegetation index

1. Introduction

In recent years, a trend has been observed in Mediterranean areas showing an increase in both the frequency and severity of adverse events related to temperature and precipitation. Extended periods of drought, episodes of extreme temperatures, and prolonged heat waves have become more common [1–6]. It is well known that long periods of low rainfall and high temperatures generate elevated rates of evapotranspiration, ultimately intensifying climatic severity [7–9].

These changes in precipitation and temperature patterns are increasingly linked to climate change [10–15]. In this scenario, water availability is reduced and is negatively affecting the volume of water reserves. At the same time, high rates of evapotranspiration are clearly harming both soil and plant moisture levels.

In the case that concerns us in this work, droughts significantly reduce the availability of water for irrigation and, consequently, soil moisture levels, which—together with high rates of evapotranspiration, as previously mentioned—cause crops to experience substantial water stress. This results in fields being abandoned, crops drying out completely, or, at best, exhibiting stunted growth that severely diminishes productivity [16–20].

 doi:10.20944/preprints202509.1149.v1

This situation is evident in Mediterranean regions that face this severe climate crisis [21], leading to fierce competition for water resources. These are complex areas where an intense struggle for water affects not only agricultural spaces independently, but also urban areas and, especially, those where both coexist [22], further aggravating the problem. In such territories, there is a coincidence: the most productive irrigated agricultural areas overlap with zones designated for urban development; here, population growth, tourism-related activities, urban expansion, and intensive irrigated agriculture all converge [23,24].

Paradoxically, irrigated crops have continued to grow, as we will demonstrate later, with subtropical crops—mainly mangoes and avocados—expanding most persistently despite being in a semi-arid environment. This has created a high demand for water, which is necessary to achieve optimal yields. This type of crop was introduced to the Mediterranean region of Europe from Central America, specifically from Mexico, about 30 years ago. In this context, these crops have become locally sourced products for the European market, highly sought after by consumers, and they fetch prices that are especially attractive for farmers. This not only explains why cultivated areas have steadily increased in the study area over recent decades, but also why this has become a way of life for many farmers; therefore, any solution must take their needs and acceptance into account.

The increasing demand for water to sustain agricultural production of these crop types has become a serious problem in these arid and semi-arid regions [25,26]. On numerous occasions, the urgent need to adopt more efficient irrigation strategies has been raised in order to ensure sustainable and economically viable production [27–31]. Conversely, water scarcity can represent a significant obstacle for farmers, which is further exacerbated during drought periods [32], as production becomes severely limited during those times [33]. In response to this shortage, groundwater pumping is often used to compensate for the lack of surface water, being, in many cases, the only alternative to offset the deficit and maintain yields [34,35]. In this context, and despite all the above, there remains an inadequate awareness regarding water scarcity and the efficient use of water resources. This has led farmers to over-irrigate, causing notable decreases in the water table, with risks of salinization and depletion [36,37].

Thus, the scope of the analysis focuses on a Mediterranean area in the south of the Iberian Peninsula. In this region, there is ongoing overexploitation of water reserves for this type of crops. Although it is evident that this is currently a difficult problem to solve, it is clear that studies analyzing it in depth, such as the one we present here, are necessary. Therefore, we want to show that, from a climatic perspective, periods of drought and high temperatures will become increasingly frequent. It is also crucial to design irrigation strategies that adapt to shortages and periods of scarcity, considering that there may be limitations in water resources at times. The frequency, amount, and distribution of irrigation must be regulated, even though these crops suffer serious dehydration damage under extreme heat and deficit irrigation conditions [38–40].

Based on the territorial evidence that illustrates the issue at hand, we propose the following objectives for analysis. First, to examine how drought is impacting the availability of water resources. Second, to analyze how water deficits affect irrigated crops, particularly subtropical crops. Third, to determine whether there is any spatial pattern in the distribution of crops that is conditioned by water scarcity. Finally, to provide reflections aimed at minimizing the problem based on the analyses carried out.

To this end, we propose a methodology that can be replicated in other territories with similar characteristics and that allows for the systematization of procedures to obtain knowledge useful to researchers interested in this field of study. At the same time, it is a methodological proposal that seeks to contribute to water sustainability in this type of agricultural crops, demonstrating that technological solutions exist to make agricultural production more efficient.

We rely on the fact that this topic has been widely developed across various lines of research. From a geographical perspective, the most compelling area is not only the study of the spatial expansion of crops or their environmental consequences, but also the application of remote sensing techniques for crop monitoring, specifically to manage their conditions through precision agriculture

 doi:10.20944/preprints202509.1149.v1

approaches [41–44]. It is also essential to understand the variable behavior of crops and to measure their evolution over time in order to achieve efficiency in the use of inputs, thus saving water resources—not only aiming for economic savings but also for more rational water use in irrigation.

Thus, the methodology first addresses the identification of the duration and magnitude of drought periods. For this, we have used the SPI (Standardized Precipitation Index) and SPEI (Standardized Precipitation-Evapotranspiration Index). In 2009, the WMO (World Meteorological Organization) recommended that countries use the SPI as the main index for meteorological drought, since it is an effective indicator for identifying, monitoring, and analyzing drought conditions [45–49]. We used these indices to define the type and intensity of drought, as they facilitated its monitoring. As is known, a drought period occurs whenever the SPI, regardless of the time scale analyzed, remains continuously negative and reaches an intensity of -1.0 or lower; the event ends when the SPI becomes positive [50]. Each drought event, therefore, has a duration defined by its beginning and end, and a different intensity for each month it persists. The SPEI index, based on the SPI, includes a temperature parameter, which allows the effect of temperature on the emergence of droughts to be considered through a basic calculation of water balance [51]. This makes it ideal for observing the impact of rising temperatures caused by climate change in regions where temperature significantly influences the effects of drought [52], such as during the Mediterranean summer season. This index quantifies the severity and temporal variability of droughts [53], with a multiscale character that is crucial for analyzing impacts on vegetation [51,54]. The advantage of using multiscalar drought indices is related to their ability to account for differences in the response times of vegetation or water reserves to conditions of water deficit [55,56].

Combining the information provided by the aforementioned indices with the use of remote sensing is fundamental for generating agronomically applicable data, broadening the scope of analysis when we rely on data collected by remote sensors with different resolutions, and therefore at different scales. It is precisely this interplay of scales that, until now, has allowed for more precise diagnostics at the crop level. However, with improvements in remote sensing systems, a single scale may be sufficient to discern parameters such as crop heterogeneity, detect problems early, or determine possible water needs [57,58]. Nonetheless, other scales remain relevant and are valuable for these types of studies, such as supplementing information with sensors installed in the soil or on UAVs that collect highly accurate, site-specific data within plantations [59]. Moreover, thanks to open access to a wide variety of remote sensor imagery, it is possible to expand the application of remote sensing techniques. There are numerous experiences and applications in different crops using products from various remote sensors [60–62].

This study utilized Sentinel imagery from the Copernicus program. Such images have been in use for some time. Many studies have employed Sentinel-2 data [63], including for the remote estimation of crop and grass chlorophyll and nitrogen content using red-edge bands on Sentinel-2 and Sentinel-3 [64], for evaluating the potential of using crop biomass [65,66], or for land cover classification using Sentinel-2A [67]. The use of this data source is determined by its utility for obtaining vegetation indices, as our interest here is in acquiring useful information about crop status. These data have proven extremely useful for analyzing crop conditions and their level of water stress, allowing us to map their distribution and the changes occurring in cultivated surfaces, which, as we will see later, are highly dependent on extreme climatic events such as drought [68]. Since there is a freely accessible image archive available from 2015 onward, it is possible to conduct time series analyses from that date. In this way, we have been able to observe the dynamics of drought effects on crops and regularly update the information [69,70]. Furthermore, a spatial resolution of 10x10 meters per pixel has been achieved, allowing for more detailed analysis and yielding excellent results [71–74]. Thanks to this, we have been able to make more precise interpretations [75,76].

As a result, we have monitored crop status in relation to periods of drought, extreme heat and heatwaves. The scientific literature supporting our study in this area is extensive. Drought analysis based on vegetation conditions has emerged as one of the strongest research topics in remote sensing [17,77,78]. Another aspect related to our work is how climatic conditions influence physiological and

 doi:10.20944/preprints202509.1149.v1

biochemical changes that reduce crop health, enabling the identification of areas with water stress [79–82], since the leaves of trees—and specifically, chlorophyll, its structure, and water content—show observable changes according to their spectral response [83–88]. Other studies confirm significant links between leaf chlorophyll and water content, canopy temperature, and tree water stress [89,90]. It has also been observed that when soil moisture falls below the drought threshold and cannot meet water demand, crop cells begin to lose water, leading to changes in morphological structure and canopy cover [91,92]. With this, we have been able to detect zones with less effective irrigation, observing reductions in greenness and water content as signs of plant stress [1,93]. Finally, the objectives of our study required the use of vegetation indices as indicators to complete the analysis, evaluating the dynamics of crop status in relation to droughts and their effects on crops [94,95], thus providing information on their health status [96–100].

The following vegetation indices were used in this study to analyze the effects of drought on crops: NDVI, NDWI, NDMI, NDDI, MSI, GNDVI [16,101–103]. Through NDVI [104], we sought to observe the response of crops to drought conditions, as it is an index widely employed in these cases [105–107], including for detecting changes in crops [108–110]. NDVI also yields good results for monitoring crop status due to the unequivocal response when crops are irrigated. As expected, the use of the NDVI index allowed us to represent the absorption of chlorophyll pigments in plants and the reflectance of vegetative matter [10,68]. This has been highly useful for measuring changes in the chlorophyll content of crop canopies [75,111,112], and we obtained a strong correlation between these changes and episodes of precipitation deficit, given that plants responded by reducing photosynthetic activity, leading NDVI values to decrease [113]. It was observed that if an area consistently shows low NDVI values, this indicates a need for irrigation to maintain or promote crop growth [36,114]. Other indices we have tested include MSI, which has helped assess crop and soil water content and stress [114,115]. NDWI and NDMI have proven sensitive to changes in the leaf water content that forms the canopy [94,116,117], allowing us to establish the relationship with soil moisture content [118].

On the other hand, this study aimed to address the intensity, geographic scope, and temporal dynamics of droughts, which largely depend on how vegetation indices are interpreted and applied [36,113,119]. The combination of indices and the classification of their values have been very important for establishing reliable indicators of crop stress, mainly due to dry conditions, allowing degrees of intensity to be defined [120]. The spatial extent of drought has been determined by examining the distribution patterns of drought values in relation to the vegetation indices applied to these crop areas [34,121].

Given that the analysis process cannot be static, we have conducted temporal monitoring of drought with the aim of understanding complete dynamics, from the beginning of the period considered (2014) until recovery after precipitation events [122]. The goal was to measure its duration and intensity through the changes observed in index values over time, thus facilitating the spatiotemporal assessment of its effects on the territory [91,123]. Therefore, a combined use of vegetation indices and drought monitoring indices was implemented [124–126]. Studies indicate that this is the best way to analyze drought and that by combining multiple data sources—including vegetation indices with hydrological or meteorological data—a more comprehensive perspective is obtained [10,113,127,128]. This approach aids the construction of multisensor models [129], which integrate various techniques to better address the complexity inherent in studying drought [53,102,130]. Drought indices can incorporate all this information: meteorological data, the status of water resources and reserves (both surface and groundwater), and vegetation indices. Altogether, this information can enhance management and irrigation techniques applied to crops with varying water needs, which is essential for measuring water use efficiency in conditions of scarcity [131–136].

 doi:10.20944/preprints202509.1149.v1

2. Materials and Methods

2.1. Study Area

The study area is classified, from a climatic standpoint, within the semi-arid Mediterranean zones, which are considered critical regions of the Mediterranean climate due to their tendency toward increasing aridity [77,137]. This includes southern Spain, located at the western edge of the Mediterranean Sea (Figure 1). The study area covers an extension of 1,023.72 km² within this region. It is particularly interesting for research given the diverse situations related to the study topic. The area is characterized by complex orography, with an altitudinal gradient exceeding 2,000 meters above sea level within just 20 km from the coast. This topography prevents cold air masses from entering and moderates winter temperatures, while conversely accentuating summer heat. Agricultural spaces are concentrated in the valleys, as the remainder of the land is mountainous, reducing the availability of arable soils. In these valleys, groundwater resources and the most fertile soils for cultivation are also located.

As previously mentioned, the study area features a typical subtropical Mediterranean climate, with an average annual temperature of 17.4°C and a maximum of 28°C, as well as an average annual precipitation of 576 mm. These temperatures are favorable for cultivating subtropical species such as mango and avocado, which require temperatures between 10°C and 30°C. Outside this range, the crop's potential yield decreases, necessitating the identification of zones that meet the required temperature thresholds. This is why the initial cultivation areas were located along coastal riverbanks, where a very mild microclimate prevails due to the presence of high mountains adjacent to a warm, continentalized sea—the Mediterranean. This setting provides protection from inland cold while also creating a sunny microenvironment on south-facing mountain slopes.

As for rainfall, it is insufficient for this type of crop, and even more so for any irrigated agriculture, since these crops require daily or near-daily irrigation on a regular schedule. For this reason, the establishment of irrigated crops in the area was made possible by the availability of surface water resources, which are hydrologically regulated by the Viñuela reservoir. In this text, we will refer to these resources as stored water, used both for agricultural irrigation and urban supply. On the other hand, dryland crops predominated until the construction of the reservoir in 1994. As is known, dryland crops in Mediterranean regions are much less demanding in terms of water, as they rely on rainfall. Since then, irrigated crops have continuously expanded, especially subtropical varieties such as avocado and mango [138]. It has already been noted that these crops require large volumes of irrigation water, which, alongside coastal tourism, creates significant pressure on the scarce available water resources [39,139,140]. For instance, in recent years, a total of 1,342 illegal infrastructures related to water extraction have been identified as a means for many farmers to increase water availability, responding to water scarcity or supply shortages due to the absence of adequate hydrological planning [141].

The irrigated area within the study region was measured at 14,372.56 hectares in 2023, according to data from the Natural Heritage Information System of Andalusia (SIPNA, acronyms in Spanish). Of this total, subtropical crops accounted for 63.59%, covering a surface area of 8,942.52 hectares. It is important to consider newly established plantations, which occupy 2,418.42 hectares (14.98% of the total irrigated area) and are not yet included in production data. Horticultural crops covered 1,585.81 hectares (11.27% of the irrigated area), citrus crops occupied 557.14 hectares (3.96%), and greenhouses covered 868.67 hectares (6.17%). As can be understood, all of these crop types require abundant water resources for their survival.

It is also important to note, especially due to its implications for water demand, that the average age of the crops is 9 years, ranging from 6 years in the youngest plantations to 20 years in the oldest. Most of these are mature, productive trees. The planting patterns used—which determine tree density—range from the traditional spacing of 8x8 m to 7x8 m, to narrower layouts in younger, primarily intensive plantations: 4x4; 4x1.5; 3x3; 3x1.5; and 2x1.5 m². For example, in one hectare (10,000 m²), for an 8x8 m grid, each tree occupies 32 m², resulting in a total of 312 trees. If the grid is

 doi:10.20944/preprints202509.1149.v1

reduced to 4x4 m—a medium-density model—each tree occupies 16 m², increasing the number to 625 trees per hectare. The plantation structure, as with any other crop, is determined by the grower, who should consider the environment and soil conditions to establish the appropriate number of seedlings.

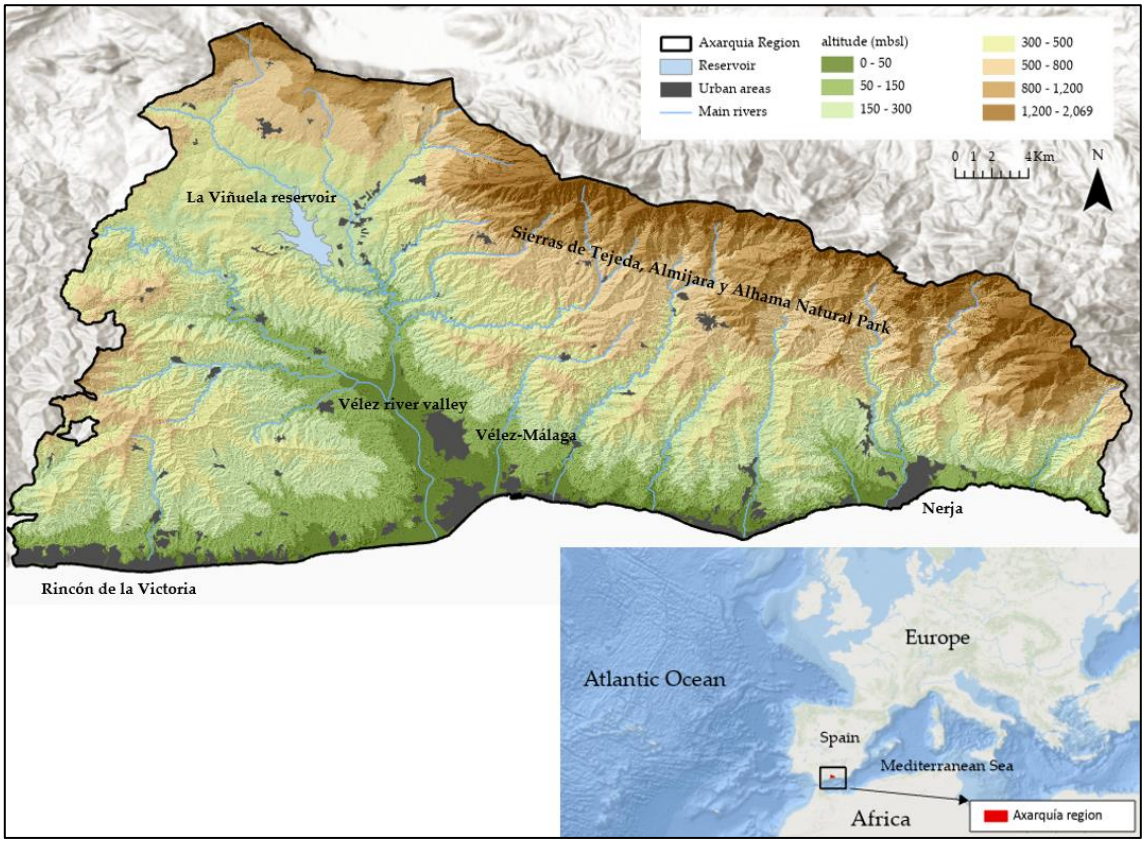

Figure 1. Location of the study area. South of Spain.

According to data collected by the authors in the field, it is evident that a sufficient and well-distributed water supply is vital for an avocado plantation to remain healthy and achieve high yields sustainably over many years. On average, an avocado tree requires approximately 110 liters of water per week, while a mango tree requires between 50 and 120 liters per day. It is important to note that the irrigation method used is drip irrigation, as this system allows water to be applied directly to the root zone and offers greater control over moisture loss under the prevailing environmental conditions of these Mediterranean semi-arid environments. However, it should be mentioned that irrigation systems largely depend on soil type; generally, there are 2–3 laterals per row of trees, with an emitter flow rate of 0.6–2.3 l/h, increasing up to 4 l/h during the hottest months, and an irrigation frequency of approximately 6 hours per day.

The estimated water needs for crops in this area are around 8,000 m³/ha per year, as calculated by local irrigation communities. Nevertheless, several factors influence the determination of these needs (climate, plantation orientation, tree age, soil type, etc.), which can even vary at the plot level. The agency responsible for water distribution, the Confederación Hidrográfica del Sur, under the Government of Spain, has set an allocation of 7,692 m³/ha for subtropical crops in the study area. This figure is clearly insufficient for growers and does not meet the water requirements of these crops, especially during periods of severe precipitation shortage. To check the availability of stored water, real-time data on reservoir volumes can be accessed through the Automatic Hydrological Information System (SAIH, acronyms in Spanish) of the Red Hidrosur (https://www.redhidrosurmedioambiente.es/saih/).

 doi:10.20944/preprints202509.1149.v1

2.2. Materials and Methods

To address the objectives of the study, we followed the scheme presented below in Figure 2, which serves as a reference for the subsequent methodological development.

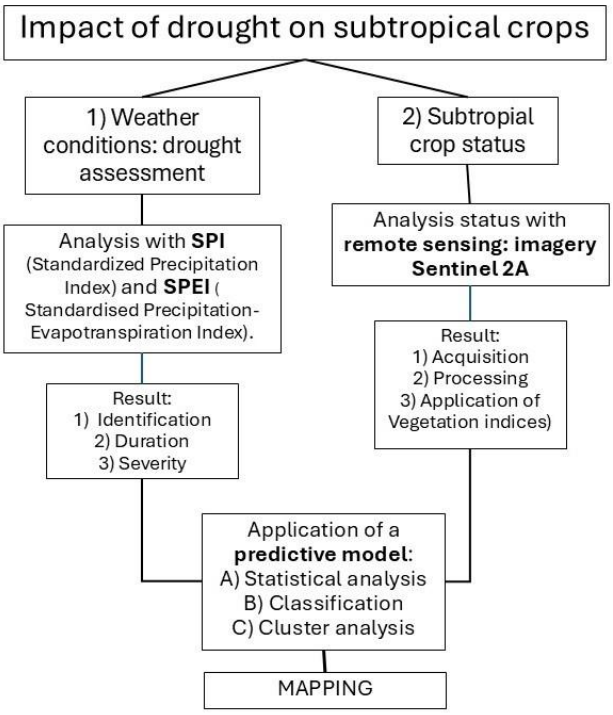

Figure 2. Methodological processes for evaluate the impact of drought on subtropical crops.

As shown in Figure 2, in order to assess the magnitude of demand pressure on water resources, we analyzed precipitation patterns using the SPI index, which helps identify meteorological drought, and the SPEI index at time scales greater than 12 months, which is used to detect hydrological drought periods and their intensity. To quantify the irrigated areas, we utilized land use information downloaded from the Andalusian Natural Heritage Information System (SIPNA, acronyms in Spanish). Based on this data, the area occupied by these types of crops was delineated. Finally, satellite images for remote sensing analysis were obtained from the Copernicus Data Space Ecosystem (Sentinel 2A). The starting date for data analysis coincides with the implementation of stored water resources in 1994 and extends to 2024 (a 30-year period) that provides sufficient perspective on the evolution of climatic conditions.

2.3. Temporal Delimitation of Drought Periods

The methodological process begins with identifying the duration and magnitude of drought using data from the SPI and SPEI indices at various time scales, along with the volume of accumulated water that supplies irrigation for subtropical crops [77]. Selecting the appropriate time scale for both indices is crucial to define the type of drought being analyzed [55,142]; therefore, monthly reservoir water values are correlated with monthly SPI and SPEI values from 1 to 48 months using Pearson's correlation. The highest correlation indicates the most suitable time scale for defining hydrological drought, since a drop in reservoir levels directly results in reduced water resources for irrigation [56,143]. Once the time scale is selected, the impact of different drought magnitudes on reservoir water levels is observed, and a linear regression is applied to confirm the prediction. Additionally, it is essential to monitor the 12-month SPEI behavior, as a longer drought period might mask a shorter wet period that is sufficient to allow a temporary recharge of reservoir water and, consequently, an increase in extractable availability [53]. Finally, to determine the drought period to

 doi:10.20944/preprints202509.1149.v1

be analyzed, it is necessary for the SPEI value to remain below -1 continuously over time [45], combined with water reserves reaching a deficit level that leads to insufficient irrigation resources.

2.4. Satellite Image Acquisition and Processing

Once the drought event is defined, available satellite images are selected for both the initial date—which indicates the crops' previous condition—and the final date, to evaluate the end state and evolution throughout the drought. The chosen image dates begin in September for two main reasons: first, to ensure that the water supplied to the crops comes exclusively from irrigation, taking advantage of the Mediterranean climate's typical summer drought [45,111,144]; and second, because this is a key stage when the fruit is reaching full development, immediately before harvesting, meaning that a lack or deficit of irrigation directly impacts crop health and reduces productivity [1,93,102]. Our analysis centers on the use of Sentinel-2 satellite imagery from ESA's Copernicus program. As is known, Sentinel-2 currently includes two active satellites (the Level 2A and Level 2B products), which, through their multispectral optical sensors, provide images across 13 spectral bands. The minimum spatial resolution is 10x10 meters (10 m/px) for most bands, with 20 m and 60 m resolution for others (see Table 1). This resolution is well suited for the objectives of our study and the geographic area under analysis.

Table 1. Spectral bands for the Sentinel-2 sensors.

Sentinel-2 bands	Sentinel-2A		Sentinel-2B		Spatial resolution (m)
	Central wavelength (nm)	Bandwidth (nm)	Central wavelength (nm)	Bandwidth (nm)	
Band 1 – Coastal aerosol	442.7	21	442.2	21	60
Band 2 – Blue	492.4	66	492.1	66	10
Band 3 – Green	559.8	36	559.0	36	10
Band 4 – Red	664.6	31	664.9	31	10
Band 5 – Vegetation red edge	704.1	15	703.8	16	20
Band 6 – Vegetation red edge	740.5	15	739.1	15	20
Band 7 – Vegetation red edge	782.8	20	779.7	20	20
Band 8 – NIR	832.8	106	832.9	106	10
Band 8A – Narrow NIR	864.7	21	864.0	22	20
Band 9 – Water vapour	945.1	20	943.2	21	60
Band 10 – SWIR – Cirrus	1373.5	31	1376.9	30	60
Band 11 – SWIR	1613.7	91	1610.4	94	20
Band 12 – SWIR	2202.4	175	2185.7	185	20

Data source: Radiometric and spectral bands for the S2 sensors of the European Space Agency (ESA). Available online: https://sentinels.copernicus.eu/web/sentinel/user-guides/sentinel-2-msi/resolutions/radiometric (accessed on: 16/06/2025).

Downloading and processing are conducted using SNAP software, specifically developed to handle imagery from the Sentinel satellites. Additionally, the Sen2Cor plugin is installed, which serves as an excellent tool for atmospheric and geometric correction of Sentinel satellite data (the Level-2A product) [53,145]. This procedure is essential for performing multitemporal image analyses and for reliably comparing spectral indices [146]. The following steps are undertaken:

1) Download Sentinel 2A and 2B satellite images at Level L1C using the "Product Library" tool for the selected dates that include our study area, which is divided into two images.
2) Atmospheric correction of the images is performed with the "Sen2Cor" tool, upgrading them from Level L1C to Level L2A to enhance visualization.

 doi:10.20944/preprints202509.1149.v1

3) Crop the images spatially and spectrally using the "Subset" tool, defining the study area and selecting the bands to be used—specifically bands 2, 3, 4, 8, and 11—to reduce data volume.
4) Standardize the spatial resolution of the spectral bands to 10 meters with the "Resampling" tool, since band 11 has a resolution of 20 meters and the rest are 10 meters.
5) Merge the two images that make up the study area with the "Mosaicking" tool, using the WGS84 projection, ortho-rectified with the Copernicus Global DEM at 30 meters and a pixel size of 10 meters.

This workflow can be implemented by building a model using the "Graph Builder" tool (Figure 3). Once the model is defined, the "Batch Processing" tool allows users to load the created model and apply it to different images simultaneously, streamlining the process.

Figure 3. Model for processing Sentinel-2 images in SNAP.

Es preciso aplicar también un proceso de verificación para el control de las calidad de las imágenes, sobre todo como es el caso, cuando se trata de estudios cuantitativos y multitemporales, ya que de ello depende la calidad de los resultados. Hemos observado que uno de los principales problemas que tiene el uso de imágenes Sentinel-2 para este tipo de estudios es el de la corrección atmosférica y de iluminación.

It is also essential to implement a verification process to ensure the quality control of the images, especially in quantitative and multitemporal studies, as the reliability of the results depends on this. One of the main challenges associated with the use of Sentinel-2 images for such studies is atmospheric and illumination correction. In Sentinel-2 products, a preliminary step before utilization involves converting radiance to apparent reflectance at the top of the atmosphere (TOA) for a flat surface. This transformation is straightforward but must be followed by a conversion from apparent reflectance to true reflectance, i.e., at the surface level (BOA, bottom of atmosphere). Variables considered in the transformation from radiance to BOA reflectance include illumination geometry, water vapor content, and aerosol optical thickness in the atmosphere. Additionally, the potential influence of clouds must be taken into account, especially cirrus or translucent clouds, which are common in semi-arid environments due to typical atmospheric conditions (surface heat and high-altitude cold). This results in persistent daytime haze when winds are absent. The quality of atmospheric correction results depends on the accuracy of available input data for these variables and effects, as well as the model applied to the radiance or TOA reflectance image [147,148].

Image correction is performed using the Sen2Cor tool, as previously mentioned. Sen2Cor is a processor for Sentinel-2, Level 2A product generation and formatting. It performs atmospheric, terrain, and cirrus corrections on Top-Of-Atmosphere (TOA) Level 1C input data, producing Bottom-Of-Atmosphere (BOA) output. Its product format is equivalent to the Level 1C User Product: JPEG 2000 images, at three different resolutions—60, 20, and 10 meters [149]. This ensures the acquisition of images free from atmospheric reflectance artifacts that could negatively affect subsequent analysis.

Another important consideration when working with time series derived from the combination of several spectral bands is the need to access each available image individually, rather than averaging images from specific periods, as this could increase statistical error in the results of vegetation indices generated in the next methodological step. Let us examine an example:

Three sequences of images within the temporal range from 2017-10-01 to 2018-01-30.

Bands: B4 and B8 from Sentinel 2A.

Reflectance values for B4: 1, 4, 3. The mean of these values is: (2+4+3)/3 = 3.

Reflectance values for B8: 2, 7, 3. The mean of these values is: (2+7+3)/3 = 4.

Calculation of the mean reflectance values for a hypothetical NDVI case:

$$\text{NDVI: } \bar{x}\ NDVI = (4-3)/(4+3) = 0.143$$

 doi:10.20944/preprints202509.1149.v1

Calculation of individual reflectance values for a hypothetical NDVI case and the mean calculated NDVI:

Sequence 1: (2-1) / (2+1) = 0.333

Sequence 2: (7-4) / (7+4) = 0.273

Sequence 3: (3-3) / (3+3) = 0

$$\bar{x}\ NDVI = (0.333 + 0.273 + 0)/(3) = 0.202$$

As observed in the previous examples, it is necessary to carry out combinatorial procedures in order to reduce the possibility of error, as even using only three images, the margin of error can be quite high. Therefore, it is advisable to access all available images within the temporal study range prior to calculating vegetation indices. With this in mind, we have performed an initial filtering of Sentinel-2A images based on several factors to avoid including data from images that could introduce noise when creating vegetation indices:

1) Images were selected for the study's temporal range: from 2015 (the earliest available images) to 2024. It was necessary to harmonize images taken before and after January 25, 2002, to ensure comparability, as changes in image processing within the Copernicus program— which began generating images with new radiometric calibration— directly affected temporal image analysis, especially when conducting comparisons of vegetation indices as in this case.
2) Images from the area of interest were chosen by selecting only the tile or tiles (100x100 km2 grid images, orthorectified in UTM/WGS84 projection) that encompass the study area, thus providing the input geometry.
3) A clip was performed using this input geometry, cropping the 100x100 km2 images to only the area corresponding to the specific crop and variety under study. This approach allows for an accurate assessment of the heterogeneity in crop evolution, minimizing interference from other crop types or varieties. Achieving data homogeneity is essential.
4) Pixels associated with water vapor (clouds) were removed, as their reflectance does not represent the surface of interest and would generate negative values when analyzing vegetation indices. To achieve this, Sentinel-2 Level-2A's QA60 band is used—see Table 2 for a simplified overview of the filtering criteria—by which a straightforward function is created for cloud masking. Technically, QA60 is not a true spectral band but rather reuses two far-infrared water vapor reflectance bands. The source bands are B10 and B11, with the QA60 service flagging, via a Boolean filter, any bits where opaque clouds are present. With this, we can assess each image, apply all previous filters, and finally apply this last step, which removes all pixels where QA60 indicates opaque clouds.
5) When applying a bitmask for QA60, each image must be processed sequentially by date, applying the cloud-masking algorithm, and saving it with its corresponding date and without clouds. If a particular image is fully cloud-covered, it is excluded from the image collection. If it is mostly clear, it is retained, and for images with a certain proportion of removed pixels, their influence will be weighted accordingly in subsequent mean calculations.

Table 2. Operation and data provided by the bands 'QA'.

Bands	Pixel size	Description
QA10	10	Always empty
QA20	20	Always empty
QA60	60	Cloud mask (1)

Available online: https://developers.google.com/earth-engine/datasets/catalog/COPERNICUS_S2_SR_(accessed on: 18/02/2025).

(1) Bitmask for QA60.
Bit 10: Opaque clouds 0: No opaque clouds.1: Opaque clouds present.
Bit 11: Cirrus clouds. 0: No cirrus clouds. 1: Cirrus clouds present.

 doi:10.20944/preprints202509.1149.v1

2.5. Image Analysis, Application of Spectral Indexes and Statistical Analysis

Once the images have been processed and corrected, the area occupied by subtropical crops is analyzed by applying various spectral indexes, which are then subjected to statistical tests to develop a model that best identifies the impact of drought events and possible irrigation deficits on these crops. The selected vegetation indexes (VI) (see Table 3) were chosen based on scientific literature because they facilitate the interpretation of crop and soil condition under drought [16,17,114]. These indexes include NDVI, GNDVI, and GCI to detect crop health and vigor [34,101,111,150], NDWI for identifying water presence [2,94], and NDDI, NDMI, and MSI to assess soil dryness and vegetation stress due to water shortages [56,94,98,118,151]. It will later be shown that not all these indexes yield the expected results when subjected to statistical analysis.

Table 3. Vegetation indexes (VI) used to analyze drought.

VI	Formula	Bands	Application
Normalized Difference Vegetation Index	NDVI = (NIR - RED) / (NIR + RED)	NDVI = (B8 – B4) / (B8 + B4)	Monitoring vegetation reduction and water stress in cultivated areas
Green Normalized Difference Vegetation Index	GNDVI = (NIR - GREEN) / (NIR + GREEN)	GNDVI = (B8 – B3) / (B8 + B3)	Similar to NDVI, it is more sensible to chlorophyll
Green Chlorophyll Index	GCI = (NIR / GREEN) - 1	GCI = (B8 / B3) -1	Identify areas with water deficiencies and monitor the immediate effects of drought on crops
Normalized Difference Water Index	NDWI = (GREEN - NIR) / (GREEN + NIR)	NDWI = (B3 – B8) / (B3 + B8)	Detect the presence of water
Normalized Difference Moisture Index	NDMI = (NIR - SWIR) / (NIR + SWIR)	NDMI = (B8 – B11) / (B8 + B11)	Detecting soil moisture and water content in vegetation
Moisture Stress Index	MSI = SWIR / NIR	MSI = B11 / B8	Identifying areas of high vulnerability to drought
Normalized Difference Drought Index	NDDI = (NDVI - NDWI) / (NDVI + NDWI)		Monitoring and assessing drought, identifies risk areas

Data source: Bibliographic references consulted that have been cited in the previous paragraph.

The calculation of the VIs is carried out using the "raster calculator" tool in ArcGIS Pro software, where the formula for each VI is entered and applied to the already processed images. Subsequently, the area of subtropical crops is delineated based on land use data from the Andalusian Natural Heritage Information System (SIPNA), and with the "extract by mask" tool in ArcGIS Pro, the results of the VI calculations are extracted, streamlining the process. With all the VIs calculated for the area of subtropical crops, a principal component analysis is performed using SPSS software. The composition of the components will identify the VIs best suited to build an effective predictive model that can explain the impact of drought and irrigation deficit on crops, further simplifying the process [152,153]. The component that explains the highest percentage of variance and is consistent with the defined objective is selected. Once the component is defined, and to verify the robustness of the results, Bartlett's test of sphericity, the KMO test, and Cronbach's alpha are applied, making the necessary adjustments that will determine the final model to be used [2,113].

2.6. Classification of Indexes, Cluster Analysis and Mapping

Next, before conducting the cluster analysis, the results obtained from the calculation of the selected vegetation indices are classified according to the following criteria:

 doi:10.20944/preprints202509.1149.v1

1) For vegetation indices focused on detecting crop health and vigor, a distinction is made between crops with low and high vegetation cover, taking into account that young plantations may be included among those with low cover.
2) For vegetation indices measuring canopy and soil moisture content, a differentiation is established between irrigated and non-irrigated crops, as well as the water stress they may experience due to a lack of water or insufficient irrigation.

To validate the robustness in the application of these criteria, scatter plots are generated, calculating both the correlation and the linear regression between the VIs. This process is carried out using SPSS software. In addition, specific literature has been consulted in which classifications are applied to VIs for different plant species [2,25,34,36,49,112,114,154].

Once the indices are classified, the images are reclassified with ArcGIS Pro software in order to perform a cluster analysis using the "multivariate clustering" tool, applying the K-medoids algorithm and the pseudo F statistic to select the optimal number of clusters [155,156]. This final cluster analysis allows for the differentiation of cultivated areas with similar characteristics and behaviors, as well as the temporal comparison of the status of subtropical crops, highlighting the most significant changes that occurred after the drought period. For this, the "compute change raster" tool is used, selecting the categorical difference method in ArcGIS Pro software. As a result, we obtain, on one hand, data that allow us to evaluate the volume and magnitude of changes experienced by the crops and, on the other, maps that make it possible to assess their spatial distribution across the territory.

Finally, for the proper application of these indices in assessing the condition of the studied crops, we have considered a series of result verification aspects:

1) Disposition, quantification, and evolution of the crop. Understanding physical aspects is essential both to comprehend how the crop responds to specific events and interventions, and to interpret monitoring results. To achieve this, a temporal sequence of RGB images is conducted. This analysis allows for observation of crop evolution and temporal variability, enabling detection of possible impacts suffered by the crop, its response to solutions or management techniques applied in the field, correlation of crop behavior in areas with different productivity, as well as the recording of this information for comparison at different times.
2) Study of crop behavior according to the different growth cycles during the same season. Throughout the production months, information is obtained to assess the state, variability, and evolution of crop vigor and water status, with the aim of detecting impacts and anomalies.
3) Crop characterization. This is carried out considering three variables: Tree Count Management, Tree Height Measurement, and Erosion Risk, with the intention of evaluating the homogeneity of the cultivated area under analysis.

3. Results

3.1. Temporal Analysis of Drought

In Mediterranean semi-arid climates, as is the case here, the alternation between dry and wet periods becomes evident when analyzing data across different time scales of the SPI and SPEI indices. This pattern is also reflected when these data are correlated with water reservoir storage levels. The shorter SPEI time scales, at 3 and 6 months, display greater variability in this alternation, while the longer time scales, from 12 to 48 months, define dry and wet periods more clearly, as the alternation appears more continuous over time. A wet period—lasting at least one year on any SPEI time scale, with values above 0—is sufficient to ensure adequate stored water, and it is even possible to maintain high reservoir levels for at least a year during wet periods, provided precipitation is abundant, with values above 1. Dry periods cause stored water reserves to decrease, and it is estimated that depletion can occur within a four-year horizon, although the actual time to depletion will depend on the previous state of the reserves and the intensity of demand.

During the years analyzed with these indices, from 1995 to 2025 (see Figure 4), several situations can be observed, with a clear correlation between stored water and precipitation volume. Other

 doi:10.20944/preprints202509.1149.v1

periods, such as those in 2005 and 2008, show reservoir levels shifting from high to very low, coinciding with a dry period which, although moderate in intensity, did not see any restrictions on irrigation water use—this is reflected across all SPEI time scales. It can be observed that dry periods have been more recurrent than wet ones, but from 2014 onwards, precipitation shortages have become more evident, leading to a prolonged dry cycle stretching to 2024 and reaching extreme intensity in current SPEI values. This is most clearly reflected in the 24-, 36-, and 48-month SPEI, while the 3-, 6-, and 12-month SPEI indicate a brief wet period in 2018. Notably, despite experiencing a more severe dry period, the rate at which water reserves have been depleted over the past ten years has been lower than in two earlier periods—1999–2000 and 2005–2008. This is explained by the implementation of water supply restrictions in order to adjust demand to the available reserves.

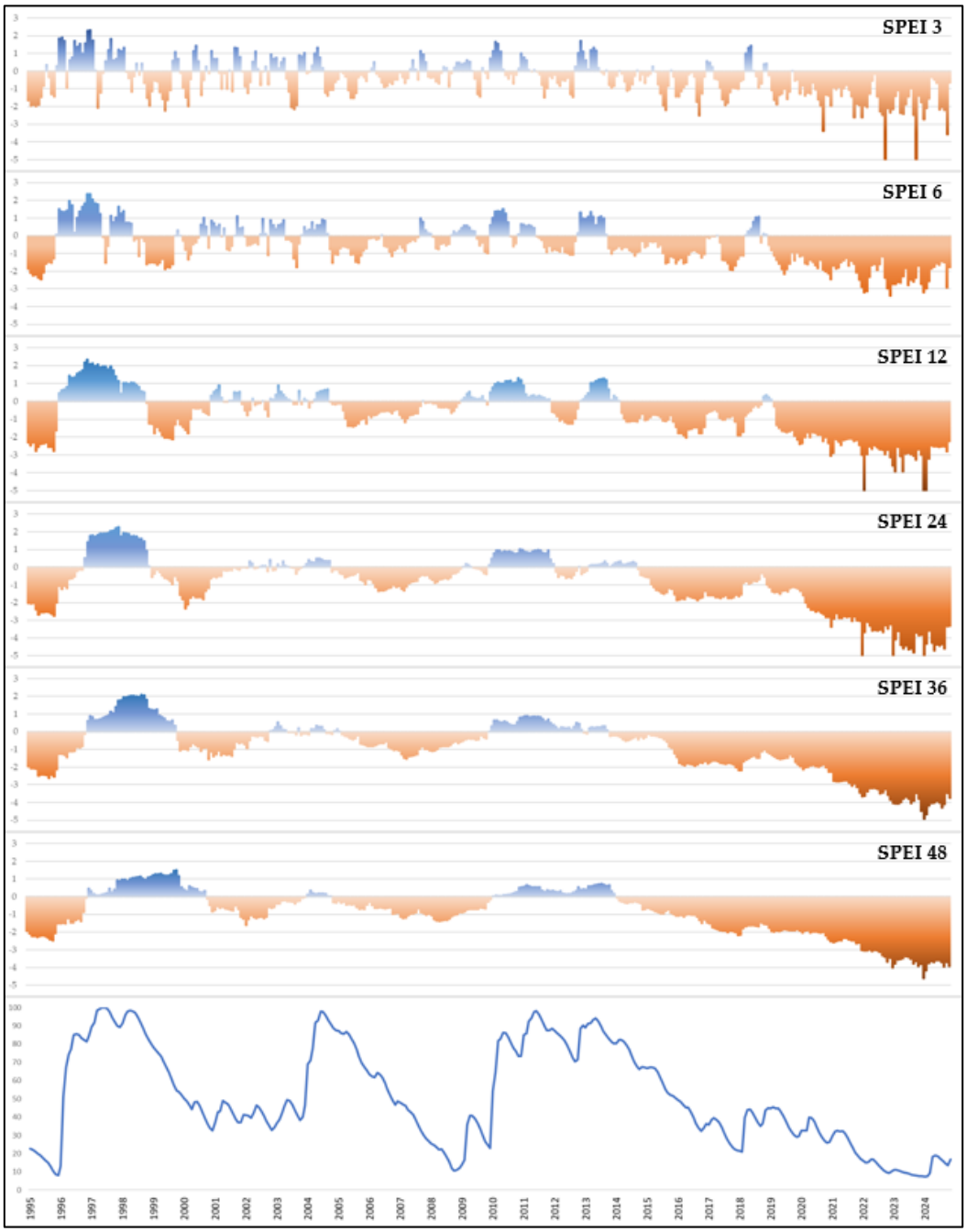

Figure 4. Graphs of the different time scales of the SPEI and the percentage of water reserve in the Viñuela reservoir during the period 1995-2024.

 doi:10.20944/preprints202509.1149.v1

The application of the Pearson test to the monthly data on reservoir water levels and the SPEI time scales (6, 12, 24, 36, and 48 months) for the period 1995–2024 (see Table 4) shows a positive, significant, and generalized correlation. The lowest value is found in SPEI 6 with 0.522, and the highest in SPEI 36 with 0.813. Although all variables show significant relationships, the values are higher in the longer SPEI time scales, indicating that this better captures the correlation with reservoir water levels. In this context, and based on the observed data, we have used two-time scales to identify the drought period: one, SPEI 36, which shows the highest correlation value, and another, SPEI 12, which indicates a shorter wet period that had not previously been detected.

Table 4. Correlation matrix of variables analysed to identify drought.

		RL		*SPEI 6*		*SPEI 12*		*SPEI 24*		*SPEI 36*		*SPEI 48*
RL	Pearson's r	—										
	p-value	—										
SPEI 6	Pearson's r	0.522	***	—								
	p-value	< .001		—								
SPEI 12	Pearson's r	0.662	***	0.854	***	—						
	p-value	< .001		< .001		—						
SPEI 24	Pearson's r	0.769	***	0.717	***	0.870	***	—				
	p-value	< .001		< .001		< .001		—				
SPEI 36	Pearson's r	0.813	***	0.613	***	0.759	***	0.929	***	—		
	p-value	< .001		< .001		< .001		< .001		—		
SPEI 48	Pearson's r	0.800	***	0.576	***	0.681	***	0.838	***	0.940	***	—
	p-value	< .001		< .001		< .001		< .001		< .001		—

*Note. * p < .05, ** p < .01, *** p < .001. RL: reservoir level (hm3). Period analysed: 1995–2024.*

The scatter plot segmented by the intensity levels of the 36-month SPEI (Figure 5), along with the following chart (Figure 6), reveals a linear correlation between drought and the volume of stored water reserves, with an R^2 of 0.6605. According to this analysis, water storage logically increases during wet periods, when SPEI 36 values are near or above 1. When SPEI–36 values are around the average, between -1 and 1, the volume of stored water is highly variable, ranging from minimum to almost maximum levels. During periods of moderate drought, with SPEI–36 values between -1 and -1.5, water reserves are around 45%. In periods of severe drought, with SPEI–36 values between -1.5 and -2, the percentage of water reserves drops to approximately 35%. Finally, in periods of extreme drought, with SPEI–36 values below -2, water reserves continue to fall, reaching only 18% availability for irrigation. Clearly, when SPEI–36 values are below -1, reservoir water reserves decrease, always remaining below 50% of capacity. Since the construction of the water storage infrastructure in 1994, SPEI–36 values have been below -1 for 43.5% of the time (Figure 6), compared to wet periods—with SPEI values above 0—which have occurred during just over 25% of the reservoir's lifespan (Figure 6). In reality, during 43.58% of the reservoir's operational life, the SPEI value has been below -1, meaning the area has experienced drought nearly half the time. Moreover, the most intense drought levels—severe and extreme—account for almost 30% of the infrastructure's lifespan, during which the average water level has been 35.74% and 18.13%, respectively.

 doi:10.20944/preprints202509.1149.v1

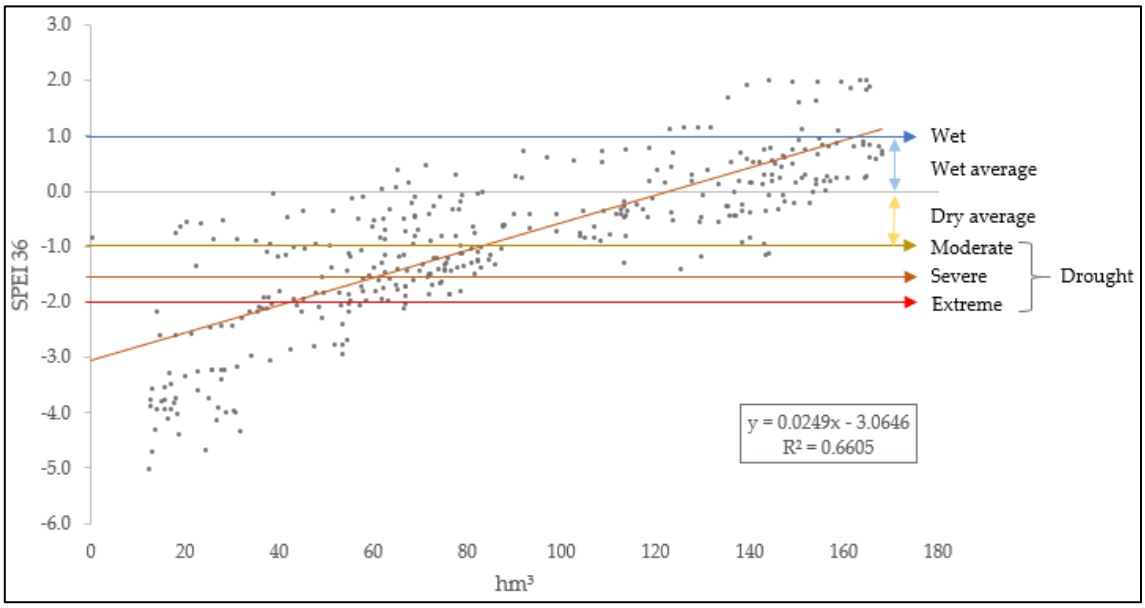

Figure 5. Scatter plot of the variables reservoir level and SPEI 36. Period analysed: 1995–2024. SPEI classification: extreme drought (< -2); severe drought (-1.5 – -1.99); moderate drought (-1 – -1.49); dry average (0 – -0.99); wet average (0.01 – 1); and wet (>1.01).

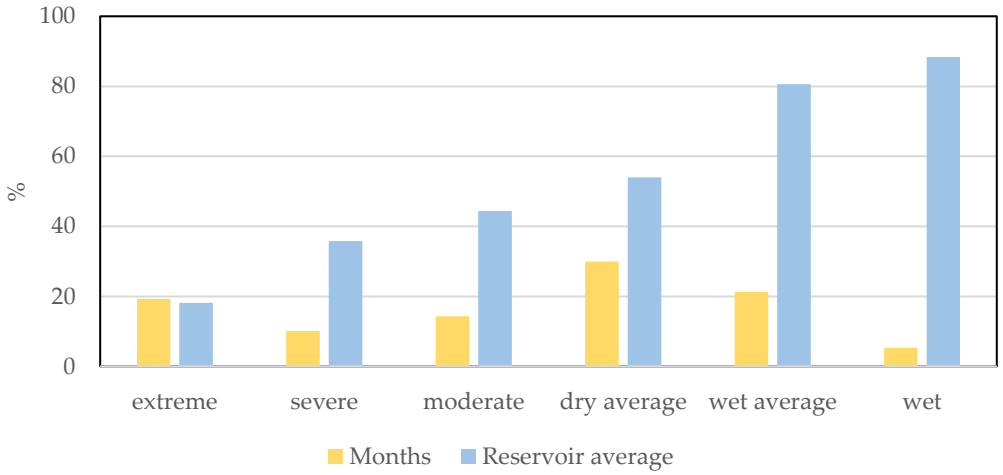

Figure 6. Duration porcentaje and average reservoir level for each SPEI 36 classification period. Period analysed: 1995–2024.

We have also analyzed the evolution of the 36-month SPEI over the past 15 years (see Figure 7), where it becomes evident that from December 2015, SPEI values drop below -1 and do not rise above this threshold again until late 2024, indicating the duration of the most severe drought period. Until November 2020, the drought intensity is considered moderate and at times severe, with values between -1 and -2, due to sporadic rainfall episodes—sometimes lasting just one day or even a few hours—that were nonetheless of high intensity. After this point, the region enters into an extreme drought period, with an almost total absence of rainfall, as the values continue descending below -2, reaching nearly -5 at their lowest point. When comparing these results to the volume of stored water (Figure 7), it can be observed that since the summer of 2013—marking the start of the dry period with values below 0—there is a progressive decline in reservoir levels, interrupted only by minor and mostly insignificant increases during winter or spring periods, which correspond to the brief precipitation events previously mentioned. This dynamic brought the stored water down to 7% of capacity by September 2023. One of the aforementioned increases stands out, as it raised reservoir

 doi:10.20944/preprints202509.1149.v1

levels by more than 20% between February and May of 2018. If we analyze the SPEI–12 data (Figure 7), we find a small masked wet period during these dates, indicating there was a rise in available reserves in the cultivated plots, which allowed the filling of private reservoirs and ponds used for supplemental irrigation, as well as recharge of the aquifers that supply the existing wells. All these factors likely reduced the demand for water from the main reservoir.For this reason, it was ultimately decided to move the start of the drought period to September 2018, spanning five years until September 2023, which coincides with the lowest reservoir levels and the latest official land use data available.

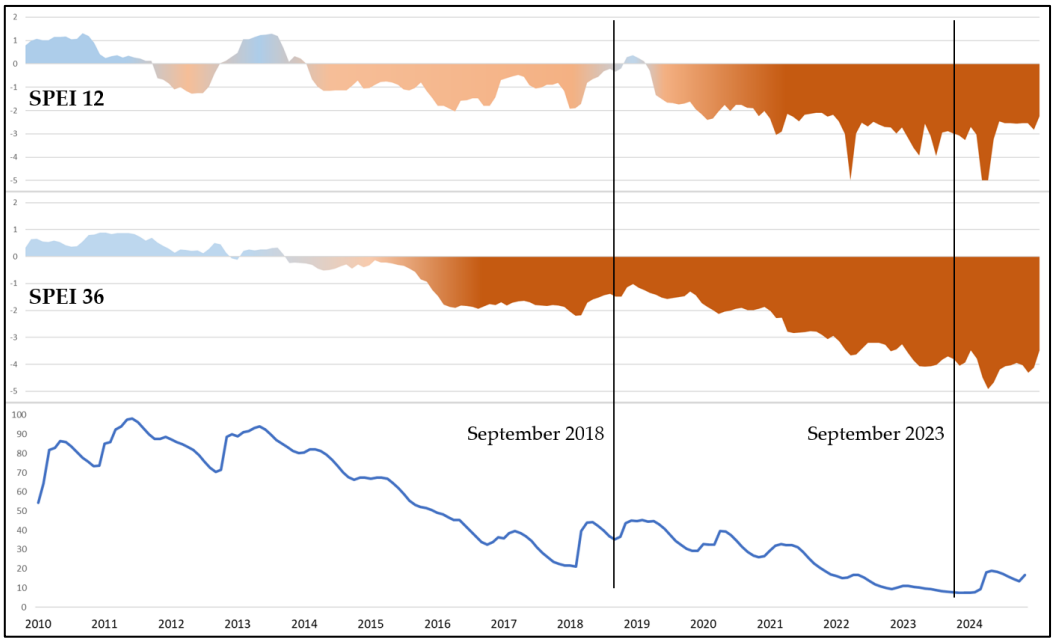

Figure 7. Evolution of SPEI with time scales of 12 and 36 months and percentage of water reserves during the period 2010-2024.

3.2. Statistical Analysis, Classification and Clustering of Spectral Indices

During the last years numerous vegetation indices have been used to make quantitative estimates of leaf area index, percent ground cover, plant height, biomass, plant population, and other parameters. Most formulae are based on ratios or linear combinations and exploit differences in the reflectance patterns of green vegetation and other covers [157–164]. Starting from this knowledge various indices are used for assessing vegetation and soil properties in this satellite remote sensing applications. We use index: NDVI, NDWI, NDMI, NDDI, MSI, GNDVI. Some indices, such as normalized difference vegetation index (NDVI) and normalized difference water index (NDWI), are capable of simply differentiating crop vitality and water stress.

In this study, the aim was to identify the contribution of each index in order to perform a combined analysis of all of them. Nevertheless, it is important to remember that this part of the methodology focuses on assessing the state of the crops according to the climatic conditions to which they have been exposed, as described in previous sections, without overlooking the different possibilities for receiving the necessary irrigation for their production and, in some cases, for their survival. It is also important to recall that planting methods, as previously explained, tend to be highly heterogeneous. Furthermore, differences are often determined by planting dates and the distinct stages of the crop cycle. For this reason, we consider it essential to know these factors in order to correctly interpret the evidence at hand. Similarly, it is necessary to have data from each of these periods to accurately display the state of the crop. The temporal resolution provided by Sentinel-2 makes it possible to address all crop stages, which are outlined below, with each stage demanding different water requirements for the trees:

 doi:10.20944/preprints202509.1149.v1

1) Planting season. Takes place from spring through early summer. Spacing begins at 4x4 m² to 8x8 m², or even 4x8 m², and when the trees grow and their canopies touch, the center tree is removed. This, of course, determines the spectral response. In addition to the planting framework, several conditions must be understood for optimal plant development: soil status, moisture conditions, and the climate balance.
2) Harvest season. Fruit is collected from November through May. Harvest usually starts in November, but only if fruit drops or if it has grown substantially. Most commonly, the harvest begins in December and ends by late April, though these dates can shift based on the year and temperature, as leaving fruit on the tree influences flowering. At this stage, it is crucial to track the overall health of the plant.
3) Pruning stage. Performed twice a year: once at the end of winter (March) and once in summer (July/August), though some growers carry out pruning in September. Notably, August is usually a critical month in most Mediterranean climate cultivation zones, as not only can the developing fruit deteriorate due to heat, but the plant itself also suffers from water stress.
4) Flowering stage. Typically occurs in spring, in March and April. In semi-arid regions, flowering coincides with rising temperatures, making it necessary to monitor conditions closely to ensure this process unfolds as desired, especially since after these months (June–July) fruit drop can increase due to heat and the small size of young fruits.
5) Fertilization period. Generally, three applications are made: one at the onset of the rainy season (late September/October) and two more every two months (December and February). It is important to monitor this process, as fertilization is often carried out indiscriminately, without considering the diverse soil conditions.

Based on the above, a statistical analysis, classification, and clustering procedure was designed for the vegetation index values. First, Pearson's test was applied to assess correlation. The indices selected for drought analysis show a high and significant correlation, except for the NDDI (see Table 5). To support this procedure, a principal component analysis (PCA) was performed, reducing the information to three components corresponding to the three initial approaches (see Table 6). The first component explains the second approach—crop moisture content and water stress—and partially covers the first approach related to vegetation structure and coverage. This component consists of four spectral indices: MSI, NDMI, NDWI, and NDVI. The most significant contributor is MSI, with a loading of 0.921, reflecting crop water stress; NDMI and NDWI follow closely, both at 0.891, indicating crop moisture content; NDVI, with a loading of 0.495, is less significant, influenced by changes in vegetation structure and coverage. This first component explains 74.7% of the variance. The second component addresses the first approach, namely vegetation structure and coverage, and comprises GNDVI, GCI, and NDVI. Here, GNDVI contributes most (0.917), measuring vegetation vigor and coverage changes (with less saturation than NDVI); GCI follows (0.875), quantifying chlorophyll content to assess crop health; and NDVI (0.855). This component adds almost 15 percentage points to the variance explained, reaching 88.9%. The third component corresponds to the third and final approach, the impact of drought, and is comprised solely of NDDI, contributing 1.0. This last component increases the cumulative variance explained by an additional 9%, reaching 98.3%. Bartlett's sphericity test results are significant at $p < .001$, supporting the adequacy of the data for analysis; however, the KMO test value is unsatisfactory at around 0.50, indicating the presence of partial correlations among some indices that should be considered to avoid bias in the results. Additionally, Cronbach's alpha was not fully reliable at 0.626, so the component composition had to be revised to improve the overall consistency.

Following exploratory data analysis, a predictive model was defined to assess the impact of drought on the crop types analyzed. Using the first two principal components and reviewing the indices to enhance model robustness and consistency, three indices were selected: NDVI, NDMI, and MSI. This selection improved the KMO value to 0.634 and Cronbach's alpha reliability to 0.913, while Bartlett's sphericity test remained significant at $p < .001$.

 doi:10.20944/preprints202509.1149.v1

Table 5. Correlation matrix of the selected spectral indices.

		NDVI		GNDVI		GCI		NDWI		NDMI		MSI		NDDI	
NDVI	Pearson's r	—													
	p-value	—													
GNDVI	Pearson's r	0.979	***	—											
	p-value	< .001		—											
GCI	Pearson's r	0.921	***	0.928	***	—									
	p-value	< .001		< .001		—									
NDWI	Pearson's r	0.824	***	0.743	***	0.772	***	—							
	p-value	< .001		< .001		< .001		—							
NDMI	Pearson's r	0.824	***	0.743	***	0.772	***	1.000	***	—					
	p-value	< .001		< .001		< .001		< .001		—					
MSI	Pearson's r	-0.785	***	-0.698	***	-0.706	***	-0.988	***	-0.988	***	—			
	p-value	< .001		< .001		< .001		< .001		< .001		—			
NDDI	Pearson's r	-0.016	*	-0.016	*	-0.011		-0.012		-0.012		0.012		—	
	p-value	0.014		0.012		0.075		0.056		0.056		0.069		—	

Note. * p < .05, ** p < .01, *** p < .001.

Table 6. Principal component análisis of the selected spectral indices.

	Component			
	1	2	3	Uniqueness
MSI	-0.921			0.00722
NDMI	0.891			0.00224
NDWI	0.891			0.00224
GNDVI		0.917		0.01958
GCI		0.875		0.06121
NDVI	0.495	0.855		0.02425
NDDI			1.000	1.34e-6

Note. 'varimax' rotation was used.

Once the composition of the model to be applied has been defined, we focus on selecting the indices that will be included in the classification for subsequent cluster analysis. It was not considered necessary to use all indices, as some produce redundant information, consistent with previous observations. The selected indices provide information that meets the model's requirements. In this way, NDVI allows the identification of cultivated areas and differentiates changes in their structure

 doi:10.20944/preprints202509.1149.v1

and coverage; NDMI indicates whether crops are being irrigated, based on canopy moisture content; and MSI reflects the degree of water stress in crops (see Table 4).

Table 7. Classification of NDVI, NDMI and MSI indexes.

Vegetation Index	Classification	Value	Description	2018 ha	2018 %	2023 ha	2023 %
NDVI	1	-1 — 0.15	uncultivated area	450.90	3.53	1,998.47	13.9
	2	0.15 — 0.30	low cover crop	2,612.02	20.43	5,887.73	41.00
	3	0.30 — 0.45	medium cover crop	2,914.94	22.80	3,954.84	27.50
	4	0.45 — 0.60	medium/high cover crop	2,538.37	19.85	2,176.69	15.14
	5	0.60 — 1	high cover crop	4,269.11	33.39	354.83	2.47
NDMI	1	-1 — 0	non-irrigated area	4,714.05	36.87	5,443.32	37.87
	2	0 — 1	irrigated area	8,071.30	63.13	8,929.24	62.13
MSI	1	0.16 — 0.90	crops without water stress	6,654.04	52.04	6,131.28	42.66
	2	0.9 — 1.3	slightly water-stressed crops	4,754.9	37.19	7,930.97	55.18
	3	1.3 — 1.9	moderate water-stressed crops	1,359.11	10.63	309.99	2.16
	4	1.9 — 2.5	extremely water-stressed crops	16.42	0.13	0.32	0.00
	5	>2.5	water	0.87	0.007	0.00	0.00

Data source: own elaboration.

Scatterplots reinforce this classification (see Figure 8). On one hand, the R^2 of the linear regression between NDMI and MSI indices is very high for both 2018 and 2023, and their distribution is very similar. This means that if we apply the value 0 to "x" in the regression equation, we obtain a value close to 1 in "y", which increases as "x" decreases. Put differently and according to the established classification, when a crop becomes irrigated, with NDMI values above 0, MSI values drop below 1, indicating an absence of water stress. On the other hand, the relationships between NDMI and MSI with NDVI are very similar; in both cases, the R^2 of the linear regression increases slightly from 2018 to 2023, accompanied by a considerable decrease in NDVI values. This suggests that NDVI is sensitive to drought, and it is important to analyze the reasons for this decline in the index values, especially since it is also occurring in irrigated crops without water stress.

Finally, a cluster analysis was carried out, resulting in seven groupings based on similar features that describe crop conditions (see Table 8). Cluster 0 encompasses all areas not under cultivation, such as roads, water ponds, small constructions, bare soils, or very young crops lacking sufficient canopy and considered bare soil. Cluster 1 includes irrigated crops without water stress and with high canopy coverage—mature, healthy crops (typically trees over 20 years old). Cluster 2 represents irrigated crops without water stress but with low canopy coverage—healthy young crops (less than 10 years old). Cluster 3 refers to high coverage crops that are insufficiently irrigated and experience water stress. Cluster 4 describes low coverage crops with minimal irrigation and water stress; these can be young crops (less than 6 years old) or mature ones with issues of canopy greenness loss, exhibiting brownish leaves. Cluster 5 is composed mainly of mature rainfed fruit trees such as almond and olive, which are sometimes found in mixed plots with subtropical crops. Finally, cluster 6 comprises non-irrigated crops with water stress and low canopy coverage, showing greater

 doi:10.20944/preprints202509.1149.v1

deterioration than those in cluster 5. Within clusters 5 and 6, some subtropical crops may be found that have recently been abandoned due to drought. It is important to note that only a portion of irrigated crops—specifically clusters 1 and 2—show no signs of water stress.

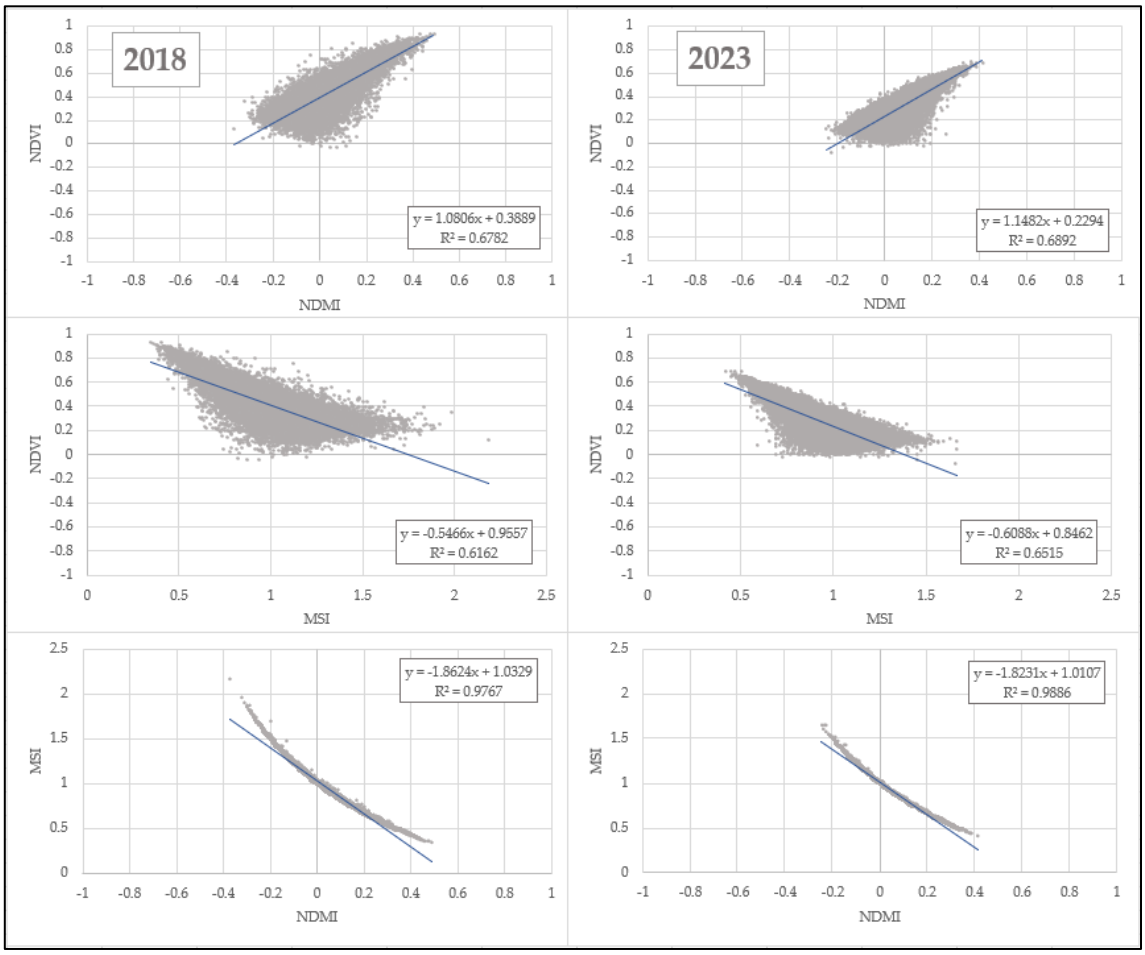

Figure 8. Scatterplot of NDVI, NDMI and MSI indices.

Table 8. Cluster analysis based on the classification of NDVI, NDMI and MSI indices.

Final cluster	NDVI	NDMI	MSI	Description
0	1	1—2	1—5	uncultivated area/young crop
1	4—5	2	1	irrigated high cover crop
2	2—3	2	1	irrigated low cover crop
3	4—5	2	2—4	irrigated water-stressed high cover crops
4	2—3	2	2—4	irrigated water-stressed low cover crops
5	4—5	1	2—4	non-irrigated water-stressed high cover crop
6	2—3	1	2—4	non-irrigated water-stressed low cover crop

Data source: own elaboration.

3.3. Mapping

The final process addressed in the methodology is the mapping of results. Table 9 shows the area occupied by each cluster in the two dates selected for analysis. From 2018 to 2023, there is an increase of just over 1,500 hectares in the total analyzed surface. In September 2018, two groups stand out above the rest: irrigated high cover crops and non-irrigated water-stressed low cover crops, representing 45.5% and 30.48% of the total, respectively. However, in September 2023, no group is

 doi:10.20944/preprints202509.1149.v1

predominant, with percentages distributed among irrigated high and low cover crops (17.55% and 24.56%, respectively), and water-stressed irrigated and non-irrigated low cover crops (17.56% and 26.36%, respectively). The uncultivated area or young crops account for 13.9%, and irrigated and non-irrigated water-stressed high cover crops have virtually disappeared.

A comparative analysis between the two dates reveals a striking decrease of almost 30 percentage points in irrigated high cover crops, as well as a less significant increase in low cover irrigated crops with and without water stress.

These trends can be explained by the varying possibilities for irrigation access. The oldest farms, considered pioneers, and those established in subsequent years, had better access to irrigation infrastructures than those created later during the rush to cultivate any available space—areas that were not always suitable and often had more precarious access to resources due to their elevation above the recognized irrigation threshold, which is set at 180 meters above sea level.

The conditions for water access in farms above this threshold and farther from main irrigation infrastructure are notably less favorable; in some cases, they relied solely on wells and small reservoirs, not on stored water infrastructures, which are demonstrably insufficient to supply crops of this kind.

Table 9. Data on the evolution of the state of subtropical crops in the Axarquia region during the drought period 2018–2023.

Cluster description	2018		2023	
	ha	%	ha	%
Uncultivated área/young crop	450.90	3.53	1,998.47	13.90
Irrigated high cover crop	5,817.10	45.50	2,523.06	17.55
Irrigated low cover crop	801.35	6.27	3,530.44	24.56
Irrigated water-stressed high cover crop	539.08	4.22	8.37	0.06
Irrigated water-stressed low cover crop	829.16	6.49	2,524.14	17.56
Non-irrigated water-stressed high cover crop	451.31	3.53	0.09	0.001
Non-irrigated water-stressed low cover crop	3,896.45	30.48	3,788.00	26.36
Total	12,785.35	100	14,372.56	100

Data source: own elaboration.

The spatial distribution of the clusters is shown in Figure 9, which illustrates how, in 2018, subtropical crops with high coverage, irrigated and healthy, can be clearly distinguished from non-irrigated crops suffering from water stress and low coverage. The former occupy the valleys of the main rivers, most notably the central/southern part of the Vélez River valley and its tributary, the Benamargosa, just downstream from the La Viñuela reservoir, which facilitates access to irrigation water. These crops also extend into the surrounding low mountain areas, mainly to the west of the Vélez River valley, where water is extracted from wells to fill reservoirs that ensure supply, making them dependent on the state of the aquifer. The latter are found in the mid-mountain zones, which are more difficult to access and farther from the valleys, where water availability is scarce or non-existent.

In 2023, after the drought period, the surface area of healthy, irrigated, high-coverage subtropical crops becomes fragmented. The same region is now also occupied by irrigated, low-coverage crops—some healthy, others suffering from water stress—mainly throughout the eastern strip of the Vélez and Benamargosa valleys, although this is a widespread process. Additionally, healthy irrigated crops are expanding into the mid-mountain areas near the coast, west of the Vélez River. Abandoned crop areas have increased and are distributed alongside non-irrigated crops, occupying the mid-mountain region distant from the valleys and to the north of the La Viñuela reservoir.

 doi:10.20944/preprints202509.1149.v1

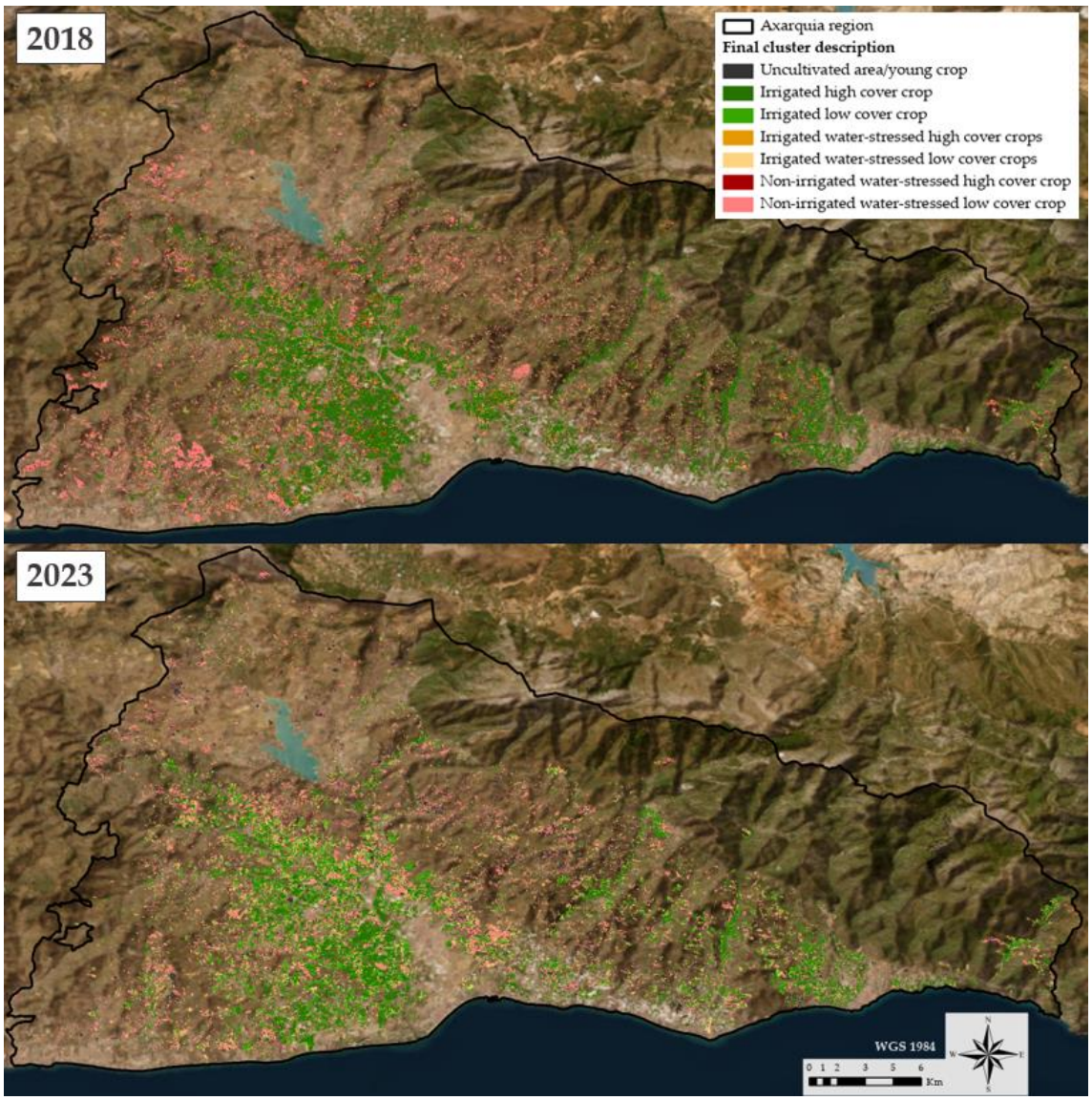

Figure 9. Map of the evolution of subtropical crops in the Axarquia region during the 2018-2023 drought period.

The changes that occurred in the clusters between 2018 and 2023 amount to a total of 9,022.79 ha, with 5,349.77 ha remaining unchanged. Table 10 lists the 10 most significant changes in terms of area, which highlight the dynamics followed by crops during this period and their condition after experiencing drought. The non-irrigated, low-coverage crops suffering from water stress in 2018 are those that underwent the greatest transformation, with 3,008.36 ha abandoned and no longer cultivated. About 1,960.13 ha of irrigated, high-coverage land in good condition experienced a reduction in coverage due to lack of irrigation. However, in 2018, 1,087.28 ha of low-coverage plantations started to be irrigated, but by 2023, these are now suffering from water stress. On the other hand, 812.44 has transitioned from non-irrigated to irrigated, although they still have low coverage and their condition has not improved. 521.40 ha that were plantations in good condition with high coverage suffered from a lack of irrigation in 2023. Another 454.68 ha stopped being irrigated, resulting in evident deterioration. Another significant change is the area occupied by 432.24 ha of irrigated, low coverage crops that have improved their condition. Lastly, 259.65 ha of older, high-coverage crops remain irrigated in 2023, while 252.95 ha of low-coverage crops are no longer irrigated and will disappear in the short or medium term. Finally, 233.66 ha of new crops that had been irrigated in 2018 are now suffering from a lack of water in 2023.

 doi:10.20944/preprints202509.1149.v1

Table 10. Main changes in the state of subtropical crop area after 5 years of drought (2018–2023).

CHANGES	2018	2023	change ha	change %
1	unchanged	unchanged	5,349.77	37.22
2	non-irrigated water-stressed low cover crop	uncultivated area	3,008.36	20.93
3	irrigated high cover crop	irrigated low cover crop	1,960.13	13.64
4	non-irrigated water-stressed low cover crop	irrigated water-stressed low cover crop	1,087.28	7.56
5	non-irrigated water-stressed low cover crop	irrigated low cover crop	812.44	5.65
6	irrigated high cover crop	irrigated water-stressed low cover crop	521.40	3.63
7	irrigated high cover crop	non-irrigated water-stressed low cover crop	454.68	3.16
8	irrigated water-stressed low cover crop	irrigated low cover crop	432.24	3.01
9	non-irrigated water-stressed high cover crop	irrigated low cover crop	259.65	1.81
10	non-irrigated water-stressed high cover crop	non-irrigated water-stressed low cover crop	252.95	1.76
11	irrigated low cover crop	irrigated water-stressed low cover crop	233.66	1.63
		Total	14,372.56	100

Data source: own elaboration.

In the spatial distribution of the main changes that occurred after the drought (see Figure 10), no specific order can be observed, as dispersion is evident, but it is possible to sense some concentration in certain more specific areas that we will try to define below: the irrigated crops that have stopped being watered, experiencing a loss of coverage and with water stress, are mainly concentrated around the valley of the Vélez River and Benamargosa, particularly in the center and east of that basin; irrigated crops with water stress are distributed throughout the region; healthy irrigated crops with loss of coverage are concentrated in the main valleys and in the lower mountains that surround them; healthy irrigated crops with increased coverage are concentrated in the southwest area of the Vélez River valley; healthy irrigated crops are concentrated in the mid/low mountains to the west of the Vélez River and Benamargosa; and the abandoned crops are concentrated more in the mid-mountain areas further away from the valleys and to the north, above the area of stored water.

 doi:10.20944/preprints202509.1149.v1

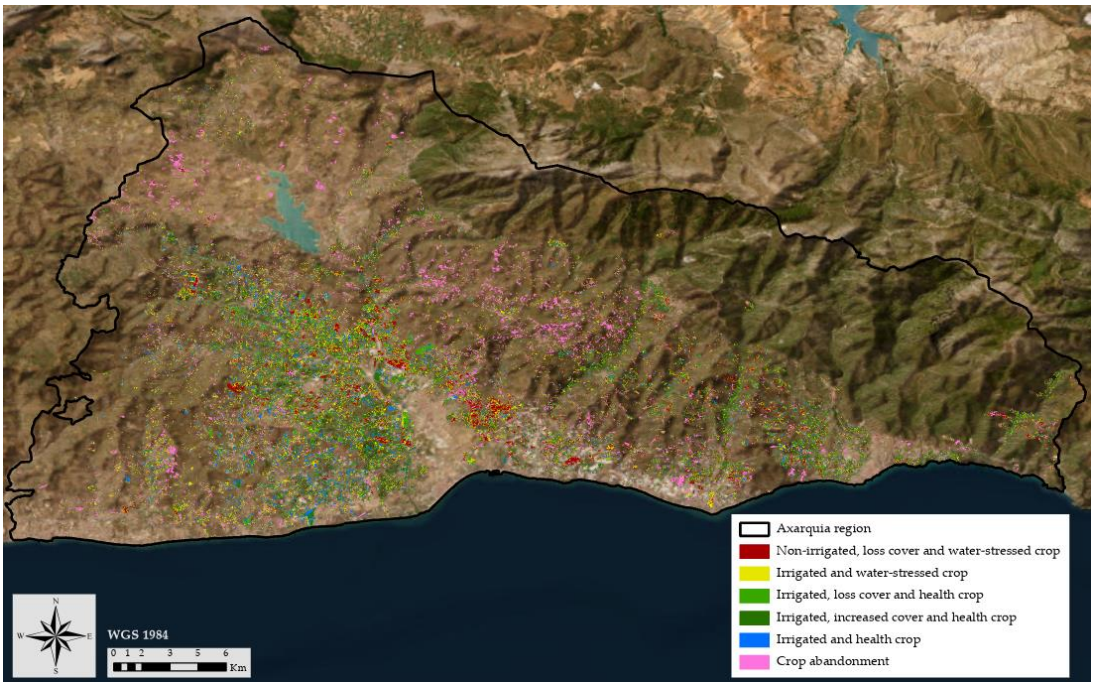

Figure 10. Map of changes in subtropical crops in the Axarquia region during the 2018-2023 drought period.

4. Discussion

As has been mentioned, the exploitation of new areas with this type of crop has become a common practice over the last few decades. This dynamic has been guided more by economic factors than by a perspective of environmental sustainability. With this work, we wanted to demonstrate this fact, in addition to the fact that in the coming decades, the conditions imposed by climate change in these territories cannot be overlooked. In these climatic domains, the scarcity of precipitation will become increasingly evident and average annual temperatures will become increasingly extreme. As a result, it will not be possible to continue planting with the current inconsistency, irrigating lands with crops that are very demanding of water. In summary, this may be the hypothesis we started from, but it was also necessary to provide a methodological proposal to support this hypothesis.

Studies indicate that the best way to analyze the complexity of the drought problem is by applying remote sensing techniques with statistical indicators, by combining various data sources, integrating vegetation indices with hydrological or meteorological data. This leads us to the construction of multisensory models, in which these various techniques are integrated to provide a better response to the complexity of the problems being analyzed.

In this work, we have once again resorted to vegetation indices in order to provide analytical elements to improve discrimination within the same type of crop in areas where differences in cover conditions occur. As is known, the use of these indices is based on their ability to discriminate plant masses by their radiometric behaviors in the different bands of the electromagnetic spectrum. We have used well-known indices such as NDVI, NDMI, or MSI. These indices have revealed significant patterns in the behavior of crops that are easily recognizable, but the study would have been incomplete if we had not analyzed the cause of the spectral response of crops, and therefore we included climatic indices such as SPI and SPEI. Various authors have pointed to the possibilities offered by combining them with vegetation indices. In this context, the analysis of the radiative transfer of leaves and canopies has been valuable for modeling and understanding the behavior of these indices. Along with this, the cause that determines the information they provide.

But perhaps there is another issue that should be considered, which we plan to analyze in future studies. We support what some authors [166] have shown that during the different stages of cultivation, the values of the indices vary, being different both in the ripening process (the color of the avocado skin changes from bright green to dark green, almost brown) and in flowering (the leaves

 doi:10.20944/preprints202509.1149.v1

are a deep green color). Like other studies, we have focused on evaluating the spectral indices in terms of their sensitivity to the biophysical parameters of vegetation and the factors affecting canopy reflectance, mainly those derived from the crop's nutritional and moisture conditions.

However, we believe that it yields good results to estimate other parameters as those outlined below.

First of all, we would highlight the estimation of the vigor of the vegetation based on the chlorophyll content in the leaves, which is an indicator of the tree's nutrition and the state of its photosynthesis. In fact, the absorption of the red band is considered optimal for estimating Chl (leaf and canopy chlorophyll) and N (canopy nitrogen), coinciding with Band 4 (664.6 -central wavelength (nm)- Sentinel-2A and 664.9, Sentinel-2B). These will be indicators that will show the state of subtropical crops, presenting high and linearly positive correlations according to the amount of chlorophyll in the leaf. For avocado vegetation covers, the average NDVI values have been around 0.601, between a maximum value of 0.890 and a minimum of 0.368 during the study period, since a typical tree of this crop, being in good condition, represents dense vegetation. In this sense, the chlorophyll content in the leaf, as the variable most directly related to the values provided by these indices, allows us to determine the differences in health status. At the same time, it allows us to reduce the interpretation that we can make solely in those areas of more leafy vegetation.

Secondly, directly related to the water availability of the plant, we would highlight the water content, either from the tree canopy in particular or from the context of the plant in general. We have made this estimation based on the main NDMI index and indirectly through the effect of water stress on LAI and chlorophyll content with reference to the NDVI and MSI indices. We estimate that vegetation indices based on shortwave infrared bands (NIR and SWIR) provide good estimates. Thus, they provide significant R values (R^2 between 0.25 and 0.60 for NDVI and 0.30 and 0.80 for NDMI), which means NDMI shows good results in its application for monitoring crop moisture, while NDVI allows for indirect estimation, only based on the effects of changes in chlorophyll due to variations in water content and leaf area index. The application of the NDWI index has helped to estimate potential evapotranspiration, as it is related to this vegetation index through leaf vigor and water stress. We can observe that some plots that showed high vigor in the NDVI, NDWI, or NDMI displayed values that predict levels of water stress in the cover. The result of applying the MSI index has yielded a good outcome at the midpoint between the two previous ones, in such a way that, while the areas of more vigorous crops are maintained, other areas with behavior closer to average or predominant values are also observed [170–172].

Thirdly, it has been interesting to observe the potential net productivity of the crop, related to the photosynthetically active radiation absorbed by the tree, especially when the leaves are horizontal and the soil is sufficiently dark, as is predominant in many areas of the study region. Some authors refer to an efficiency factor for each tree, although indirectly, green and dry biomass can be estimated from NDVI, GNDVI, and MSI, but in this case, different adjustments must be made for the results to be good [173,174].

Another aspect to consider is the LAI index, which shows a positive association with NDVI, GNDVI, and MSI, especially when the specimens are not too leafy and do not completely cover the ground, allowing for differentiation of the degree of green cover. Otherwise, with high values (above 4, mainly), NDVI becomes saturated, but MSI remains more stable. On the other hand, although indirectly, we can estimate the green biomass that will be determined by the age of the tree and its percentage of green cover, since a healthy adult tree shows a very clear response, while areas with growing specimens or greater water stress show less leaf vigor and lower canopy density [175–181].

In fifth place and considering that this work is carried out in semi-arid Mediterranean environments, the analysis of the amount of water received by the plant canopy is fundamental, because it is obviously directly related to the vigor of the tree. However, in these areas, we find a certain lag between precipitation and the response of the vegetation cover, primarily due to its irregularity, not only in time but also in its volume. Very related to this is the potential evapotranspiration in these environments due to the high temperatures we have already mentioned

 doi:10.20944/preprints202509.1149.v1

and inversely related to the vegetation indices analyzed through leaf vigor and the water stress that the tree presents, mainly from May to September. This is a crucial time as the tree needs to receive the necessary water contributions, coinciding with a high evapotranspiration; to which it should be added that it is in a process of preparing for flowering, making the need for hydration and nutrient supply fundamental for the good harvest of the following season. Consequently, after a dry hydrological year or a prolonged period of drought, farmers have had to make extraordinary water contributions so that the tree is not affected.

Finally, we want to emphasize the importance of conducting an analysis of phenological dynamics, and for this we have followed the seasonal evolution of the indices (temporal variability) and considered the characteristic factors of these cycles, which we have termed cultivation stages. The results have shown differences in the behavior of the crop, although there is also a clear correlation depending on its phenological stage. This has represented an advancement in the recognition of the crop because it allows for the identification and characterization, among other aspects, of diseases, with the indices being able to detect disorders in the expected behavior [182–185].

5. Conclusions

In this section, we will focus on it in two ways. One, in terms of the objective we had set at the beginning being fulfilled, but with some nuances. We started with the aim of demonstrating that the behavior of the analyzed crops is fundamentally dependent on the irrigation they have received, which we understand has been demonstrated. To some extent, this may seem logical: more irrigation leads to better condition. However, here are some nuances. Excessive watering does not yield good results in trees; they respond better to continuous watering, but in smaller quantities. This fact is not a problem in itself, except that during drought periods, watering days are less frequent and spaced farther apart in time. At this point, the condition of the plant begins to deteriorate and the harvest production decreases. This situation produces a reaction from farmers which is to increase irrigation times to prevent plant deterioration. If this course of action is taken during periods of drought, it will directly depend on stored water and its own water resources such as wells or reservoirs, leading to their depletion.

On the other hand, as a second aspect, there is still no awareness that planting areas need to be adapted to the available water resources, and there is the belief that these are inexhaustible; fundamentally the resources coming from aquifers, since the amounts extracted by this means are not exactly quantifiable like the resources coming from stored water, which leads to a depletion of these resources.

It is necessary to have studies like the one we present to help stakeholders become aware of the situation that can be generated by climate change, with severe droughts and prolonged high temperatures, which can become increasingly common in the semi-arid climates of Mediterranean areas.

Author Contributions: Conceptualization, D.C. and B.G.; methodology, D.C.; software, D.C.; validation, B.G., D.C. and J.S.; formal analysis, D.C..; investigation, D.C. and B.G.; resources, D.C.; data curation, D.C. and B.G.; writing—original draft preparation, D.C. and B.G.; writing—review and editing, D.C., B.G. and J.D.; visualization, D.C.; supervision, B.G. and J.D.; project administration, B.G.; funding acquisition, B.G. All authors have read and agreed to the published version of the manuscript.

Funding: This research was funded by Counseling of University, Research and Innovation, Government of Andalusia. Call for the Procedure of Granting Applied Research Projects and/or Technological Development Projects, Interdisciplinary and Intersectoral to Research Groups, within the Framework of the II Own Research, Transfer and Scientific Dissemination Plan. Vice-Rectorate of Research and Transfer, University of Malaga. Code: HUM776-G-FEDER. The APC was funded by partial funding for open access charge: University of Malaga and Consortium of University Libraries of Andalusia (CBUA, for its initials in Spanish).

 doi:10.20944/preprints202509.1149.v1

Data Availability Statement: The data presented in this study are available on request from the corresponding author.

Conflicts of Interest: The authors declare no conflicts of interest.

Abbreviations

The following abbreviations are used in this manuscript:

BOA	Bottom of Atmosphere
ESA	European Space Agency
GNDVI	Green Normalized Difference Vegetation Index
GSI	Grain Size Index
KMO	Kaiser-Meyer-Olkin method
LAI	Leaf Area Index.
MSI	Moisture index
NDDI	Normalized Difference Drought Index
NDMI	Normalized Difference Moisture Index
NDVI	Normalized Difference Vegetation Index
NDW1	Normalized Difference Water Index
SAIH	Sistema Automático de Información Hidrológica
SNAP	Sentinel Application Platform
SPEI	Standardised Precipitation-Evapotranspiration Index
SPI	Standardized Precipitation Index
SIPNA	Sistema de Información sobre el Patrimonio Natural de Andalucía
SPSS	Statistical Package for the Social Sciences
TOA	Top of Atmosphere
WMO	World Meteorological Organization

References

1. Gosling, S. N., & Arnell, N. W. A global assessment of the impact of climate change on water scarcity. *Climatic Change* **2016**, *134*, 371–385. https://doi.org/10.1007/s10584-013-0853-x
2. Hoerling, M., Eischeid, J., Perlwitz, J., Quan, X., Zhang, T., & Pegion, P. On the increased frequency of Mediterranean drought. *Journal of climate* **2012**, *25*(6), 2146–2161. https://doi.org/10.1175/JCLI-D-11-00296.1
3. Sousa, P. M., Trigo, R. M., Aizpurua, P., Nieto, R., Gimeno, L., & Garcia-Herrera, R. Trends and extremes of drought indices throughout the 20th century in the Mediterranean. *Natural Hazards and Earth System Sciences* **2011**, *11*(1), 33–51. https://doi.org/10.5194/nhess-11-33-2011
4. Le, T.S.; Harper, R.; Dell, B. Application of Remote Sensing in Detecting and Monitoring Water Stress in Forests. *Remote Sens*. **2023**, *15*, 3360. https://doi.org/10.3390/rs15133360
5. Carella, A.; Bulacio Fischer, P.T.; Massenti, R.; Lo Bianco, R. Continuous Plant-Based and Remote Sensing for Determination of Fruit Tree Water Status. *Horticulturae* **2024**, *10*, 516. https://doi.org/10.3390/horticulturae10050516
6. Vicente-Serrano, S. M., Lopez-Moreno, J. I., Beguería, S., Lorenzo-Lacruz, J., Sanchez-Lorenzo, A., García-Ruiz, J. M., Espejo, F. Evidence of increasing drought severity caused by temperature rise in southern Europe. *Environmental Research Letters* **2014**, *9*(4), 044001. https://doi.org/10.1088/1748-9326/9/4/044001
7. Salas-Martínez Fernando, Valdés-Rodríguez Ofelia Andrea, Palacios-Wassenaar Olivia Margarita, Márquez-Grajales Aldo, Rodríguez-Hernández Leonardo Daniel. Methodological estimation to quantify drought intensity based on the NDDI index with Landsat 8 multispectral images in the central zone of the Gulf of Mexico. *Frontiers in Earth Science* **2023**, *11*, 1–13. https://doi.org/10.3389/feart.2023.1027483

 doi:10.20944/preprints202509.1149.v1

8. Jonathan Spinoni, Paulo Barbosa, Alfred De Jager, Niall McCormick, Gustavo Naumann, Jürgen V. Vogt, Diego Magni, Dario Masante, Marco Mazzeschi, A new global database of meteorological drought events from 1951 to 2016, *Journal of Hydrology: Regional Studies* **2019**, *22*, 100593. https://doi.org/10.1016/j.ejrh.2019.100593.
9. Francisco José Del-Toro-Guerrero, Thomas Kretzschmar, Precipitation-temperature variability and drought episodes in northwest Baja California, México, *Journal of Hydrology: Regional Studies* **2020**, 27, 2020, 100653. https://doi.org/10.1016/j.ejrh.2019.100653.
10. Kaoutar Mounir, Isabelle La Jeunesse, Haykel Sellami, Abdessalam Elkhanchoufi. Spatiotemporal analysis of drought occurrence in the Ouergha catchment, Morocco[J]. *AIMS Environmental Science*, **2023**, *10*(3): 398-423. https://doi.org/10.3934/environsci.2023023
11. G. Legesse, K.V. Suryabhagavan. Remote sensing and GIS based agricultural drought assessment in East Shewa Zone. Ethiopia. *Tropical Ecology* **2014**,*55*(3), 349–363. https://www.researchgate.net/publication/239791588_Remote_sensing_and_GIS_based_agricultural_drought_assessment_in_East_Shewa_Zone_Ethiopia
12. Ruiz-Sinoga, J. D., Garcia-Marin, R., Gabarron-Galeote, M. A., & Martinez-Murillo, J. F. Analysis of dry periods along a pluviometric gradient in Mediterranean southern Spain. *International Journal of Climatology* **2012**, *32*(10). https://doi.org/10.1002/joc.2376
13. Rodríguez Díaz, J. A., Weatherhead, E. K., Knox, J. W., & Camacho, E. Climate change impacts on irrigation water requirements in the Guadalquivir River basin in Spain. *Regional Environmental Change* **2007**, 7, 149–159. https://doi.org/10.1007/s10113-007-0035-3
14. FAOSTAT (2016) Food and Agriculture Organization of the United Nations (FAO). FAOSTAT Database. http://faostat.fao.org/site/291/default.aspx (accessed on 06/08/2025)
15. European Environment Agency Climate change, impacts and vulnerability in Europe 2016 An indicator-based report 2017. https://doi.org/10.2800/534806 (accessed on 06/08/2025)
16. Ergene, Emine & Balcik, Filiz & Şanlı, F. Trends analysis of agricultural drought in central anatolian basin, Turkey. *The International Archives of the Photogrammetry, Remote Sensing and Spatial Information Sciences* **2024**. XLVIII-4/W9-2024. 141-148. 10.5194/isprs-archives-XLVIII-4-W9-2024-141-2024. DOI:10.5194/isprs-archives-xlviii-4-w9-2024-141-2024
17. Li, T.; Zhong, S. Advances in Optical and Thermal Remote Sensing of Vegetative Drought and Phenology. *Remote Sens*. **2024**, *16*, 4209. https://doi.org/10.3390/rs16224209.
18. Schillinger, W. F., Schofstoll, S. E., & Alldredge, J. R. Available water and wheat grain yield relations in a Mediterranean climate. *Field Crops Research* **2008**, *109*(1–3), 45–49. https://doi.org/10.1016/j.fcr.2008.06.008
19. Austin, R. B., Cantero-Martınez, C., Arrúe, J. L., Playán, E., & Cano-Marcellán, P. Yield–rainfall relationships in cereal cropping systems in the Ebro River valley of Spain. *European Journal of Agronomy* **1998**, *8*(3–4), 239–248. https://doi.org/10.1016/S1161-0301(97)00063-4
20. Li, Z., Zhou, T., Zhao, X., Huang, K., Wu, H., & Du, L. Diverse spatiotemporal responses in vegetation growth to droughts in China. *Environmental Earth Sciences* **2016**, *75*, 1–13. https://doi.org/10.1007/s12665-015-4781-0
21. Intergovernmental Panel on Climate Change (IPCC). Climate Change 2021 – The Physical Science Basis: Working Group I Contribution to the Sixth Assessment Report of the Intergovernmental Panel on Climate Change. Cambridge University Press; 2023. https://www.ipcc.ch/report/ar6/wg1/ (accessed on 06/08/2025)
22. Rosa, L., Chiarelli, D. D., Rulli, M. C., Dell'Angelo, J., & D'Odorico, P. Global agricultural economic water scarcity. *Science Advances* **2020,** *6*(18), eaaz6031. DOI: 10.1126/sciadv.aaz6031

 doi:10.20944/preprints202509.1149.v1

23. Ramos, R. Y., Romero, Ó. C., Camacho, V. F., & Delgado, M. T. The bubble of subtropical crops and the water collapse in the Axarquía. In Gabinete de Estudios de la Naturaleza de la Axarquía (GENA), Vélez-Málaga (Spain), 2020. https://euroweeklynews.com/2024/02/24/the-subtropical-bubble-impacting-axarquias-water-crisis/. (accessed on 06/08/2025)
24. Garau, E., Vila-Subirós, J., & Palom, A. R. Agua, turismo y servicios de los ecosistemas: el ciclo hidroturístico en la cuenca mediterránea. In Challenges and opportunities of a world in transition. An interpretation from Geography, 1st ed.; Escribano J., Peñarrubia M.P., Serrano J., Asins S. (Eds.): Tirant lo Blanc, Spain, 2020, Volume 1, pp. 251–264. https://www.researchgate.net/publication/344375258_Agua_turismo_y_servicios_de_los_ecosistemas_el_ciclo_hidroturistico_en_la_cuenca_mediterranea (accessed on 06/08/2025)
25. Ibrahim, G.R.F., Rasul, A. & Abdullah, H. Assessing how irrigation practices and soil moisture affect crop growth through monitoring Sentinel-1 and Sentinel-2 data. *Environ Monit Assess* **2023**, *195*, 1262. https://doi.org/10.1007/s10661-023-11871-w
26. Ma, C., Johansen, K., & McCabe, M. F. Monitoring irrigation events and crop dynamics using Sentinel-1 and Sentinel-2 time series. *Remote Sensing* **2022**, *14*(5), 5. https://doi.org/10.3390/rs14051205
27. Farid, H. U., Khan, Z. M., Shakoor, A., Mubeen, M., Ayub, H. U., Kanwar, R. M. A., & Bilal, M. (2022). Water Resources in Relation to Climate Change. In: Jatoi, W.N., Mubeen, M., Ahmad, A., Cheema, M.A., Lin, Z., Hashmi, M.Z. (eds). Building Climate Resilience in Agriculture. Springer, Cham., 145-166. https://doi.org/10.1007/978-3-030-79408-8_10.
28. Davarpanah, R., & Ahmadi, S. H. Modeling the effects of irrigation management scenarios on winter wheat yield and water use indicators in response to climate variations and water delivery systems. *Journal of Hydrology* **2021**, *598*, 126269. https://doi.org/10.1016/j.jhydrol.2021.126269
29. Kharrou, M. H., Simonneaux, V., Er-Raki, S., Le Page, M., Khabba, S., & Chehbouni, A. Assessing irrigation water use with remote sensing-based soil water balance at an irrigation scheme level in a semi-arid region of Morocco. *Remote Sensing* **2021**, *13*(6), 1133. https://doi.org/10.3390/rs13061133
30. Zuazo, V. H. D., García-Tejero, I. F., Rodríguez, B. C., Tarifa, D. F., Ruiz, B. G., & Sacristán, P. C. Deficit irrigation strategies for subtropical mango farming. A review. *Agronomy for sustainable development* **2021**, *41*(1), 13. https://doi.org/10.1007/s13593-021-00671-6
31. Bastiaanssen, W. G., Molden, D. J., & Makin, I. W. Remote sensing for irrigated agriculture: examples from research and possible applications. *Agricultural water management* **2000,** *46*(2), 137–155. https://doi.org/10.1016/S0378-3774(00)00080-9
32. FAO. Agricultural Value Chain Study in Iraq—Dates, Grapes, Tomatoes and Wheat. Bagdad, 2021. https://iraqieconomists.net/en/wp-content/uploads/sites/3/2021/04/FAO-Study-Iraq-Agriculture.pdf (accessed on 06/08/2025).
33. Fahad, S., Bajwa, A. A., Nazir, U., Anjum, S. A., Farooq, A., Zohaib, A., ... & Huang, J. Crop production under drought and heat stress: plant responses and management options. *Frontiers in Plant Science* **2017**, *8*, 1147. https://doi.org/10.3389/fpls.2017.01147
34. Hadri, A., Saidi, M.E.M. & Boudhar, A. Multiscale drought monitoring and comparison using remote sensing in a Mediterranean arid region: a case study from west-central Morocco. *Arab J Geosci* **2021**, *14*, 118. https://doi.org/10.1007/s12517-021-06493-w
35. Van Dam, J. C., Singh, R., Bessembinder, J. J. E., Leffelaar, P. A., Bastiaanssen, W. G. M., Jhorar, R. K., ... & Droogers, P. Assessing options to increase water productivity in irrigated river basins using remote sensing and modelling tools. *Water resources development* **2006**, *22*(1), 115–133. DOI:10.1080/07900620500405734

 doi:10.20944/preprints202509.1149.v1

36. Gaznayee, H.A.A.; Zaki, S.H.; Al-Quraishi, A.M.F.; Aliehsan, P.H.; Hakzi, K.K.; Razvanchy, H.A.S.; Riksen, M.; Mahdi, K. Integrating Remote Sensing Techniques and Meteorological Data to Assess the Ideal Irrigation System Performance Scenarios for Improving Crop Productivity. *Water* **2023**, *15*, 1605. https://doi.org/10.3390/w15081605
37. Alfarrah, N.; Walraevens, K. Groundwater Overexploitation and Seawater Intrusion in Coastal Areas of Arid and Semi-Arid Regions. *Water* **2018**, *10*, 143. https://doi.org/10.3390/w10020143
38. Moreno Ortega, G. Yield and fruit quality of avocado trees under different regimes of water supply in the subtropical coast of Spain. *Agricultural Water Management* **2019**, *221*, 192–201. https://doi.org/10.1016/j.agwat.2019.05.001
39. Ozelkan, E., Chen, G., & Ustundag, B. B. Multiscale object-based drought monitoring and comparison in rainfed and irrigated agriculture from Landsat 8 OLI imagery. *International Journal of Applied Earth Observation and Geoinformation* **2016**, *44*, 159–170. https://doi.org/10.1016/j.jag.2015.08.003
40. Ceccato, P.; Flasse, S.; Tarantola, S.; Jacquemoud, S.; Grégoire, J.-M. Detecting vegetation leaf water content using reflectance in the optical domain. *Remote Sens. Environ*. **2001**, *77*, 22–33. https://doi.org/10.1016/S0034-4257(01)00191-2.
41. Duan, T., Chapmana, S.C., Guob, Y., Zhenga, B. Dynamic monitoring of NDVI in wheat agronomy and breeding trials using an unmanned aerial vehicle. *Field Crops Research* **2017**, *210*, 71–80. https://doi.org/10.1016/j.fcr.2017.05.025
42. Xiao, X., Boles, S., Frolking, S., Salas, W., Moore III, B., Li, C., He, L., Zhao, R. Observation of flooding and rice transplanting of paddy rice fields at the site to landscape scales in China using vegetation sensor data. *International Journal of Remote Sensing* **2002**, *23*(15), 3009-3022. https://doi.org/10.1080/01431160110107734.
43. Jiang, X.; Fang, S.; Huang, X.; Liu, Y.; Guo, L. Rice Mapping and Growth Monitoring Based on Time Series GF-6 Images and Red-Edge Bands. *Remote Sens*. **2021**, *13*, 579. https://doi.org/10.3390/rs13040579.
44. Cheng, S.J.; Bohrer, G.; Steiner, A.L.; Hollinger, D.Y.; Suyker, A.; Phillips, R.P.; Nadelhoffer, K.J. Variations in the influence of diffuse light on gross primary productivity in temperate ecosystems. *Agricultural and Forest Meteorology* **2015**, *201*, 98–110. https://doi.org/10.1016/j.agrformet.2014.11.002.
45. Hayes, M., M. Svoboda, N. Wall y M. Widhalm. The Lincoln Declaration on Drought Indices: universal meteorological drought index recommended. *Bulletin of the American Meteorological Society* **2011**, *92*, 485–488. https://doi.org/10.1175/2010BAMS3103.1
46. World Meteorological Organization. User guide on the standardized precipitation index (OMM-No 1090), Ginebra, 2012. https://library.wmo.int/viewer/39629?medianame=wmo_1090_en_#page=1&viewer=picture&o=bookmarks&n=0&q= (accessed on 06/08/2025).
47. Rostami, E., Fattahi, M.H., Razmkhah, H.(2015) Drought forecasting using ArtificialNeural Network; Case study: Kohgilooye andBoyer Ahmad, Faculty of agriculture, Marv-dasht Islamic Azad University, Marvdasht, Iran. https://doi.org/10.21203/rs.3.rs-989454/v1
48. McKee, T.B., Doesken, N.J. and Kleist, J. The Relationship of Drought Frequency and Duration to Time Scales. 8th Conference on Applied Climatology, Anaheim, 17-22 January 1993, 179–184.
49. Vicente-Serrano, S.M., S. Begueria y J.I. Lopez-Moreno. A multi-scalar drought index sensitive to global warming: the Standardized Precipitation Evapotranspiration Index. *Journal of Climate* **2010**, *23*, 1696–1718. https://doi.org/10.1175/2009JCLI2909.1

 doi:10.20944/preprints202509.1149.v1

50. Alahacoon, N., & Edirisinghe, M. A comprehensive assessment of remote sensing and traditional based drought monitoring indices at global and regional scale. *Geomatics, Natural Hazards and Risk* **2022**, *13*(1), 762–799. https://doi.org/10.1080/19475705.2022.2044394
51. Mullapudi, A., Vibhute, A.D., Mali, S. et al. A review of agricultural drought assessment with remote sensing data: methods, issues, challenges and opportunities. *Appl Geomat*. **2023**, *15*, 1–13. https://doi.org/10.1007/s12518-022-00484-6
52. Beguería, S., Vicente-Serrano, S.M., Reig, F. and Latorre, B. Standardized precipitation evapotranspiration index (SPEI) revisited: parameter fitting, evapotranspiration models, tools, datasets and drought monitoring. *Int. J. Climatol*. **2014**, *34*, 3001–3023. https://doi.org/10.1002/joc.3887
53. Vicente-Serrano, S.M.; Gouveia, C.; Camarero, J.J.; Beguería, S.; Trigo, R.; López-Moreno, J.I.; Azorín-Molina, C.; Pashoa, E.; Lorenzo-Lacruz, J.; Revuelto, J.; Morán-Tejeda, E. and Sanchez-Lorenzo, A. Response of vegetation to drought time-scales across global land biomes. *PNAS* **2013**, *110*, 52–57. https://doi.org/10.1073/pnas.1207068110
54. Khaled Hazaymeh, Quazi K. Hassan. Remote sensing of agricultural drought monitoring: A state of art review[J]. *AIMS Environmental Science*, **2016**, *3*(4): 604–630. https://doi.org/10.3934/environsci.2016.4.604
55. Alizadeh MR, Nikoo MR. A fusion-based methodology formeteorological drought estimation using remote sensing data. *Remote Sens Environ* **2018**, *211*, 229–247. https://doi.org/10.1016/j.rse.2018.04.001
56. Niemeyer, S. New drought indices. Options Méditerranéennes. Série A: Séminaires Méditerranéens **2008**, *80*, 267–274. https://projects.iamz.ciheam.org/medroplan/zaragoza2008/Sequia2008/Session3/S.Niemeyer.pdf (accessed on 06/08/2025).
57. Haghverdi, A.; Leib, B.; Washington-Allen, R.; Wright, W.C.; Ghodsi, S.; Grant, T.; Zheng, M.; Vanchiasong, P. Studying Crop Yield Response to Supplemental Irrigation and the Spatial Heterogeneity of Soil Physical Attributes in a Humid Region. *Agriculture* **2019**, *9*(2), 43. https://doi.org/10.3390/agriculture9020043.
58. He, L.; Wang, R.; Mostovoy, G.; Liu, J.; Chen, J.M.; Shang, J.; Liu, J.; McNairn, H.; Powers, J. Crop Biomass Mapping Based on Ecosystem Modeling at Regional Scale Using High Resolution Sentinel-2 Data. *Remote Sens*. **2021**, *13*, 806. https://doi.org/10.3390/rs13040806.
59. Li, L.; Zhou, X.; Longqian, Ch.; Longgao, Ch.; Yu, Z.; Liu, Y. Estimating Urban Vegetation Biomass fromSentinel-2A Image Data. *Forests* **2020**, *11*, 125. https://doi.org/10.3390/f11020125.
60. Baret, F.; Fourty, T. Estimation of leaf water content and specific leaf weight from reflectance andtransmittance measurements. *Agronomie* **1997**, *17* (9-10), 455–464. https://hal.inrae.fr/hal-02696088.
61. Maneta, M.P.; Cobourn, K.; Kimball, J.S.; He, M.; Silverman, N.L.; Chaffin, B.C.; Ewing, S.; Ji, X.; Maxwell, B. A satellite-driven hydro-economic model to support agricultural water resources management. *Environmental Modelling & Software* **2020**, *134*, 104836. https://doi.org/10.1016/j.envsoft.2020.104836.
62. Shen, M.; Tang, Y.; Chen, J.; Zhu, J.; Zheng, Y. Influences of temperature and precipitation before the growing season on spring phenology in grasslands of the central and eastern Qinghai-Tibetan Plateau. *Agricultural and Forest Meteorology* **2011**, *151*(12), 1711-1722. https://doi.org/10.1016/j.agrformet.2011.07.003.
63. Bartold, M.; Wróblewski, K.; Kluczek, M.; Dąbrowska-Zielińska, K.; Goliński, P. Examining the Sensitivity of Satellite-Derived Vegetation Indices to Plant Drought Stress in Grasslands in Poland. *Plants* **2024**, *13*, 2319. https://doi.org/10.3390/plants13162319
64. Tian, Z., Jin, S., Cun, L., Wen, Ch. Potential Bands of Sentinel-2A Satellite for Classification Problems in Precision Agriculture. *International Journal of Automation and Computing* **2019**, *16*(1), 16–26. https://doi.org/10.1007/s11633-018-1143-x.

 doi:10.20944/preprints202509.1149.v1

65. The Sentinel-2 Atmospheric Correction Problem. INTA Copernicus Relay. Available online: https://www.inta.es/INTA/en/blogs/copernicus/BlogEntry_1509095468013# (accessed on 24/03/2025).
66. Zhanga, H.K., Roya, D.P., Yana, L., Lia, Z., Huanga, H., Vermoteb, E., Skakunb, S., Rogerb, J. C. Characterization of Sentinel-2A and Landsat-8 top of atmosphere, surface, and nadir BRDF adjusted reflectance and NDVI differences. *Remote Sensing of Environment* **2018**, *215*, 482–494. https://doi.org/10.1016/j.rse.2018.04.031.
67. Sen2cor: Science Toolbox Exploitation Platform. Available online: http://step.esa.int/main/snap-supported-plugins/sen2cor/ (accessed on 24/03/2025).
68. Radočaj, D.; Jurišić, M.; Gašparović, M. The Role of Remote Sensing Data and Methods in a Modern Approach to Fertilization in Precision Agriculture. *Remote Sens.* **2022**, *14*, 778. https://doi.org/10.3390/rs14030778
69. Parelius, E.J. A Review of Deep-Learning Methods for Change Detection in Multispectral Remote Sensing Images. *Remote Sens.* **2023**, *15*, 2092. https://doi.org/10.3390/rs15082092
70. Pham, MP., Nguyen, K.Q., Vu, G.D. et al. Drought risk index for agricultural land based on a multi-criteria evaluation. *Model. Earth Syst. Environ.* **2022**, *8*, 5535–5546. https://doi.org/10.1007/s40808-022-01376-9
71. Phiri, D.; Simwanda, M.; Salekin, S.; Nyirenda, V.R.; Murayama, Y.; Ranagalage, M. Sentinel-2 Data for Land Cover/Use Mapping: A Review. *Remote Sens.* **2020**, *12*, 2291. https://doi.org/10.3390/rs12142291
72. David J. Mulla, Twenty-five years of remote sensing in precision agriculture: Key advances and remaining knowledge gaps. *Biosystems Engineering* **2013**, *114*, 2013, Pages 358–371, https://doi.org/10.1016/j.biosystemseng.2012.08.009
73. Páscoa, P.; Gouveia, C.M.; Russo, A.C.; Bojariu, R.; Vicente-Serrano, S.M.; Trigo, R.M. Drought Impacts on Vegetation in Southeastern Europe. *Remote Sens.* **2020**, *12*, 2156. https://doi.org/10.3390/rs12132156
74. Mukherjee, S., Mishra, A., & Trenberth, K. E. Climate change and drought: a perspective on drought indices. *Current climate change reports* **2018**, *4*, 145–163. https://doi.org/10.1007/s40641-018-0098-x
75. C.M. Gouveia, R.M. Trigo, S. Beguería, S.M. Vicente-Serrano, Drought impacts on vegetation activity in the Mediterranean region: An assessment using remote sensing data and multi-scale drought indicators. *Global and Planetary Change* **2017**, *151*, 15–27, https://doi.org/10.1016/j.gloplacha.2016.06.011.
76. Harry West, Nevil Quinn, Michael Horswell, Remote sensing for drought monitoring & impact assessment: Progress, past challenges and future opportunities, *Remote Sensing of Environment* **2019**, *232*, 2019, https://doi.org/10.1016/j.rse.2019.111291.
77. Lisar, S.Y.S.; Motafakkerazad1, R.; Hossain, M.M.; Rahman, I.M.M. Water Stress in Plants: Causes, Effects and Responses In Water Stress; Rahman, I.M.M., Hasegawa, H., Eds.; IntechOpen: London, UK, 2012. https://doi.org/10.5772/39363
78. Laskari, M.; Menexes, G.; Kalfas, I.; Gatzolis, I.; Dordas, C. Water Stress Effects on the Morphological, Physiological Characteristics of Maize (Zea mays L.), and on Environmental Cost. *Agron. J.* **2022**, *12*, 2386. https://doi.org/10.3390/AGRONOMY12102386
79. Anderson, L.O.; Malhi, Y.; Aragao, L.E.O.C.; Ladle, R.; Arai, E.; Barbier, N.; Phillips, O. Remote sensing detection of droughts in Amazonian forest canopies. *New Phytol.* **2010**, *187*, 733–750. http://dx.doi.org/10.1111/j.1469-8137.2010.03355.x
80. Eitel, J.U.H.; Gessler, P.E.; Smith, A.M.S.; Robberecht, R. Suitability of existing and novel spectral indices to remotely detect water stress in Populus spp. *For. Ecol. Manag.* **2006**, *229*, 170–182. https://doi.org/10.1016/j.foreco.2006.03.027

 doi:10.20944/preprints202509.1149.v1

81. Jaleel, C.A.; Manivannan, P.; Wahid, A.; Farooq, M.; Al-Juburi, H.J.; Somasundaram, R.; Panneerselvam, R. Drought Stress in Plants: A Review on Morphological Characteristics and Pigments Composition. *Int. J. Agric. Biol.* **2009**, *11*, 100–105. https://research-repository.uwa.edu.au/en/publications/drought-stress-in-plants-a-review-on-morphological-characteristic#:~:text=Jaleel%2C%20C.%20A.%2C%20Manivannan%2C%20P.%2C%20Wahid%2C%20A.%2C%20Farooq%2C,International%20Journal%20of%20Agriculture%20and%20Biology%2C%2011%2C%20100-105. (accessed on 24/03/2025).
82. Gausman, H.W. Reflectance of leaf components. *Remote Sens. Environ.* **1977**, *6*, 1–9. https://doi.org/10.1016/0034-4257(77)90015-3
83. Zhang, F.; Zhou, G. Estimation of vegetation water content using hyperspectral vegetation indices: A comparison of crop water indicators in response to water stress treatments for summer maize. *BMC Ecol.* **2019**, *19*, 12. https://doi.org/10.1186/s12898-019-0233-0
84. Coops, N.; Stone, C.; Culvenor, D.S.; Chisholm, L.A.; Merton, R.N. Chlorophyll content in eucalypt vegetation at the leaf and canopy scales as derived from high resolution spectral data. *Tree Physiol.* **2003**, *23*, 23–31. https://doi.org/10.1007/978-3-540-93962-7_16
85. Curran, P.J.; Dungan, J.L.; Gholz, H.L. Exploring the relationship between reflectance red edge and chlorophyll content in slash pine. *Tree Physiol.* **1990**, *7*, 33–48. https://doi.org/10.1016/0034-4257(92)90136-8
86. Farooq, M.; Wahid, A.; Kobayashi, N.; Fujita, D.; Basra, S.M.A. Plant drought stress: effects, mechanisms and management. *Agron. Sustain. Dev.* **2009**, *29*, 185–212. https://doi.org/10.1051/agro:2008021
87. Pirzad, A.; Shakiba, M.R.; Zehtab-Salmasi, S.; Mohammadi, S.A.; Darvishzadeh, R.; Samadi, A. Effect of water stress on leaf relative water content, chlorophyll, proline and soluble carbohydrates in Matricaria chamomilla L. J. *Med. Plants Res.* **2011**, *5*, 2483–2488. https://doi.org/10.5897/JMPR.9000503
88. Curran, P.J. Remote Sensing of Foliar Chemistry. *Remote Sens. Environ.* **1989**, *30*, 271–278. https://doi.org/10.1016/0034-4257(89)90069-2
89. Qin, Q.; Wu, Z.; Zhang, T.; Sagan, V.; Zhang, Z.; Zhang, Y.; Zhang, C.; Ren, H.; Sun, Y.; Xu, W.; et al. Optical and Thermal Remote Sensing for Monitoring Agricultural Drought. *Remote Sens.* **2021**, *13*, 5092. https://doi.org/10.3390/rs13245092.
90. Enquist, B. J., & Ebersole, J. J. Effects of Added Water on Photosynthesis of Bistorta vivipara: The Importance of Water Relations and Leaf Nitrogen in Two Alpine Communities, Pikes Peak, Colorado, U.S.A. *Arctic and Alpine Research* **1994**, *26*(1), 29–34. https://doi.org/10.2307/1551873
91. Xiao, C.; Wu, Y.; Zhu, X. Evaluation of the Monitoring Capability of 20 Vegetation Indices and 5 Mainstream Satellite Band Settings for Drought in Spring Wheat Using a Simulation Method. *Remote Sens.* **2023**, *15*, 4838. https://doi.org/10.3390/rs15194838
92. Viswambharan, S., Kumaramkandath, I.T. & Tali, J.A. A geospatial approach in monitoring the variations on surface soil moisture and vegetation water content: a case study of Palakkad District, Kerala, India. *Environ Earth Sci* **2022**, *81*, 494. https://doi.org/10.1007/s12665-022-10611-6
93. Qiaoyun Xie, Jadu Dash, Alfredo Huete, Aihui Jiang, Gaofei Yin, Yanling Ding, Dailiang Peng, Christopher C. Hall, Luke Brown, Yue Shi, Huichun Ye, Yingying Dong, Wenjiang Huang, Retrieval of crop biophysical parameters from Sentinel-2 remote sensing imagery. *International Journal of Applied Earth Observation and Geoinformation* **2019**, *80*, 187–195, https://doi.org/10.1016/j.jag.2019.04.019.
94. Berner, Logan T.; Beck, Pieter S. A.; Bunn, Andrew Godard; Lloyd, Andrea H.; and Goetz, Scott J., "High-Latitude Tree Growth and Satellite Vegetation Indices: Correlations and Trends in Russia and Canada (1982-2008)". *Environmental Sciences Faculty and Staff Publications*. **2011**, *8*, 1–13. https://cedar.wwu.edu/esci_facpubs/8

95. Anderegg Jonas, Yu Kang, Aasen Helge, Walter Achim, Liebisch Frank, Hund Andreas. Spectral Vegetation Indices to Track Senescence Dynamics in Diverse Wheat Germplasm. *Frontiers in Plant Science* **2020**, *10*. https://doi.org/10.3389/fpls.2019.01749
96. Aya Ferchichi, Ali Ben Abbes, Vincent Barra, Imed Riadh Farah. Forecasting vegetation indices from spatio-temporal remotely sensed data using deep learning-based approaches: A systematic literature review, *Ecological Informatics* **2022**, *68*, 101552. https://doi.org/10.1016/j.ecoinf.2022.101552.
97. Bannari, A., Morin, D., Bonn, F. and Huete, A. R. A review of vegetation indices. *Remote Sensing Reviews* **1995**, *13*(1), 95–120. https://doi.org/10.1080/02757259509532298
98. Lang Qiao, Weijie Tang, Dehua Gao, Ruomei Zhao, Lulu An, Minzan Li, Hong Sun, Di Song, UAV-based chlorophyll content estimation by evaluating vegetation index responses under different crop coverages. *Computers and Electronics in Agriculture*, **2022**, *196*, 106775. https://doi.org/10.1016/j.compag.2022.106775.
99. V. W. Muriga, B. Rich, F. Mauro, A. Sebastianelli and S. L. Ullo, "A Machine Learning Approach to Long-Term Drought Prediction Using Normalized Difference Indices Computed on a Spatiotemporal Dataset," IGARSS 2023 - 2023 IEEE International Geoscience and Remote Sensing Symposium, Pasadena, CA, USA, 2023, pp. 4927–4930, https://doi.org/10.1109/IGARSS52108.2023.10282592
100. Wenzhe Jiao, Lixin Wang, Matthew F. McCabe. Multi-sensor remote sensing for drought characterization: current status, opportunities and a roadmap for the future. *Remote Sensing of Environment*. **2021**, *256*. 112313. https://doi.org/10.1016/j.rse.2021.112313
101. Gautam, D.; Pagay, V. A Review of Current and Potential Applications of Remote Sensing to Study the Water Status of Horticultural Crops. *Agronomy* **2020**, *10*, 140. https://doi.org/10.3390/agronomy10010140
102. Compton J. Tucker, Red and photographic infrared linear combinations for monitoring vegetation. *Remote Sensing of Environment* **1979**, *8*, 127–150, https://doi.org/10.1016/0034-4257(79)90013-0.
103. C.M. Rulinda, A. Dilo, W. Bijker, A. Stein, Characterising and quantifying vegetative drought in East Africa using fuzzy modelling and NDVI data. *Journal of Arid Environments* **2012**, *78*, 169–178. https://doi.org/10.1016/j.jaridenv.2011.11.016.
104. Lebrini, Youssef & Benabdelouahab, Tarik & Boudhar, Abdelghani & Htitiou, Abdelaziz & Hadria, R. & Lionboui, Hayat. (2019). Farming systems monitoring using machine learning and trend analysis methods based on fitted NDVI time series data in a semi-arid region of Morocco. Proc. SPIE 11149, Remote Sensing for Agriculture, Ecosystems, and Hydrology XXI, 111490S (21 October 2019). https://doi.org/10.1117/12.2532928
105. Gaikwad, S.V., Vibhute, A.D., Kale, K.V. Development of NDVI Prediction Model Using Artificial Neural Networks. In: Santosh, K., Hegadi, R., Pal, U. (eds) Recent Trends in Image Processing and Pattern Recognition. RTIP2R 2021. *Communications in Computer and Information Science* **2022**, 1576. Springer, Cham. https://doi.org/10.1007/978-3-031-07005-1_32
106. Gu, Y., J. F. Brown, J. P. Verdin, and B. Wardlow. A five-year analysis of MODIS NDVI and NDWI for grassland drought assessment over the central Great Plains of the United States. *Geophys. Res. Lett.* **2007**, *34*, L06407. https://doi.org/10.1029/2006GL029127
107. Gholinia, A.; Abbaszadeh, P. Agricultural Drought Monitoring: A Comparative Review of Conventional and Satellite-Based Indices. *Atmosphere* **2024**, *15*, 1129. https://doi.org/10.3390/atmos15091129
108. Drori, Ron & Dan, Harel & Sprintsin, Michael & Sheffer, Efrat. Precipitation-Sensitive Dynamic Threshold: A New and Simple Method to Detect and Monitor Forest and Woody Vegetation Cover in Sub-Humid to Arid Areas. *Remote Sensing*. **2020**, *12*, 1231. https://doi.org/10.3390/rs12081231

109. Shahin Solgi, Seyed Hamid Ahmadi, Sabine Julia Seidel, Remote sensing of canopy water status of the irrigated winter wheat fields and the paired anomaly analyses on the spectral vegetation indices and grain yields, *Agricultural Water Management* **2023**, *280*, 108226. https://doi.org/10.1016/j.agwat.2023.108226.
110. Benabdelouahab, T., Balaghi, R., Hadria, R., Lionboui, H., Minet, J., & Tychon, B. Monitoring surface water content using visible and short-wave infrared SPOT-5 data of wheat plots in irrigated semi-arid regions. *International Journal of Remote Sensing* **2015**, *36*(15), 4018–4036. Doi: 10.1080/01431161.2015.1072650
111. Kumar, V., Sharma, K.V., Pham, Q.B. et al. Advancements in drought using remote sensing: assessing progress, overcoming challenges, and exploring future opportunities. *Theor Appl Climatol*, **2024**, *155*, 4251–4288 (2024). https://doi.org/10.1007/s00704-024-04914-w
112. Qader SH, Dash J, Atkinson PM. Forecasting wheat and barley crop production in arid and semi-arid regions using remotely sensed primary productivity and crop phenology: A case study in Iraq. *Sci Total Environ.* **2018**, *1*(613–614), 250–262. https://doi.org/10.1016/j.scitotenv.2017.09.057
113. Hadi H. Jaafar & Farah A. Ahmad. Crop yield prediction from remotely sensed vegetation indices and primary productivity in arid and semi-arid lands. *International Journal of Remote Sensing* **2015**, *36*(18), 4570–4589, https://doi.org/10.1080/01431161.2015.1084434
114. Gao, B.C. NDWI—A Normalized Difference Water Index for Remote Sensing of Vegetation Liquid Water from Space. *Remote Sensing of Environment* **1996**, *58*, 257–266. https://doi.org/10.1016/S0034-4257(96)00067-3
115. Serrano, J.; Shahidian, S.; Marques da Silva, J. Evaluation of Normalized Difference Water Index as a Tool for Monitoring Pasture Seasonal and Inter-Annual Variability in a Mediterranean Agro-Silvo-Pastoral System. *Water* **2019**, *11*, 62. https://doi.org/10.3390/w11010062
116. Das, A.C.; Noguchi, R.; Ahamed, T. An Assessment of Drought Stress in Tea Estates Using Optical and Thermal Remote Sensing. *Remote Sens.* **2021**, *13*, 2730. https://doi.org/10.3390/rs13142730
117. Mishra AK, Singh VP. Drought modeling – A review. *J Hydro* **2011**, *l403*, 157–175. https://doi.org/10.1016/j.jhydrol.2011.03.049
118. Sazib N, Mladenova I, Bolten J. Leveraging the Google EarthEngine for Drought Assessment Using Global Soil Moisture Data. *Remote Sens* **2018**, *10*, 1265. https://doi.org/10.3390/rs10081265
119. Vicente-Serrano SM, Domínguez-Castro F, Reig F et al. Aglobal drought monitoring system and dataset based on ERA5 reanalysis: A focus on crop-growing regions. *Geosci Data J.* **2023**, *10*, 505–518. https://doi.org/10.1002/gdj3.178
120. Lai P, Zhang M, Ge Z et al (2020) Responses of Seasonal Indicators Extreme Droughts in Southwest China. *Remote Sens.* **2020**, *12*, 818. https://doi.org/10.3390/rs12050818
121. Diaz V, Corzo Perez GA, Van Lanen HAJ et al. An approachto characterise spatio-temporal drought dynamics. *Adv Water Resour* **2020**, *137*, 103512. https://doi.org/10.1016/j.advwatres.2020.103512
122. Sharafi L, Zarafshani K, Keshavarz M et al. Drought risk assess-ment: Towards drought early warning system and sustainable environment in western Iran. *Ecol Indic.* **2020**, *114*, 106276. https://doi.org/10.1016/j.ecolind.2020.106276
123. Rehman MA, Seth D. Investigation and modeling of electric vehicle enablers (EVE) for successful penetration in context to India: mitigating the effect of urban sprawl on transportation. *Environ Sci Pollut Res.* **2023**, *30*, 107118–107137. https://doi.org/10.1007/s11356-023-26022-4
124. Van Ginkel M, Biradar C. Drought Early Warning in Agri-Food Systems. *Climate* **2021**, *9*, 134. https://doi.org/10.3390/cli9090134

125. Tavazohi, Elena & Ahmadi Nadoushan, Mozhgan. (2018). Assessment of drought in the Zayandehroud basin during 2000–2015 using NDDI and SPI indices. Fresenius Environmental Bulletin. 27. https://www.researchgate.net/publication/324802483_Assessment_of_drought_in_the_Zayandehroud_basin_during_2000-2015_using_NDDI_and_SPI_indices (accessed on 24/03/2025)
126. McKee, T. B., Doesken, N. J., & Kleist, J. Drought Monitoring with Multiple Time Scales. In Proceedings of the Ninth Conference on Applied Climatology 1995, 233–236. Dallas,TX: American Meteorological Society. https://doi.org/10.1109/INFCOM.1996.493342
127. Salcedo-Sanz, Sancho & Ghamisi, Pedram & Piles, Maria & Werner, M. & Cuadra, Lucas & Moreno, Alvaro & Izquierdo-Verdiguier, Emma & Muñoz, Jordi & Mosavi, Amir & Camps-Valls, Gustau. Machine Learning Information Fusion in Earth Observation: A Comprehensive Review of Methods, Applications and Data Sources. *Information Fusion.* **2020**, *63*, 256–272. https://doi.org/10.1016/j.inffus.2020.07.004
128. Liu, Y., Zhu, Y., Ren, L., Yong, B., Singh, V. P., Yuan, F., ... & Yang, X. On the mechanisms of two composite methods for construction of multivariate drought indices. *Science of the Total Environment* **2019**, *647*, 981–991. https://doi.org/10.1016/j.scitotenv.2018.07.273
129. Dutta, D., Kundu, A., Patel, N.R., Saha, S.K.,Siddiqui, A.R. (2015) Assessment of agricul-tural drought in Rajasthan (India) using remotesensing derived Vegetation Condition Index(VCI) and Standardized Precipitation Index (SPI). *The Egyptian Journal of Remote Sensingand Space Sciences* **2015**, *18*, 53–63. https://doi.org/10.1016/j.ejrs.2015.03.006
130. Wenzhe Jiao, Chao Tian, Qing Chang, Kimberly A. Novick, Lixin Wang, A new multi-sensor integrated index for drought monitoring. *Agricultural and Forest Meteorology* **2019**, *268*, 74–85, https://doi.org/10.1016/j.agrformet.2019.01.008.
131. AghaKouchak, A., Farahmand, A., Melton, F. S., Teixeira, J., Anderson, M. C., Wardlow, B. D., & Hain, C. R. Remote sensing of drought: Progress, challenges and opportunities. *Reviews of Geophysics* **2015**, *53*(2), 452–480. https://doi.org/10.1002/2014RG000456
132. Van Loon, A. F., Stahl, K., Di Baldassarre, G., Clark, J., Rangecroft, S., Wanders, N., Gleeson, T., Van Dijk, A. I. J. M., Tallaksen, L. M., Hannaford, J., Uijlenhoet, R., Teuling, A. J., Hannah, D. M., Sheffield, J., Svoboda, M., Verbeiren, B., Wagener, T., and Van Lanen, H. A. J.: Drought in a human-modified world: reframing drought definitions, understanding, and analysis approaches. *Hydrol. Earth Syst. Sci*. **2016,** *20*, 3631–3650. https://doi.org/10.5194/hess-20-3631-2016
133. Vicente-Serrano, S. M., Peña-Gallardo, M., Hannaford, J., Murphy, C., Lorenzo-Lacruz, J., Dominguez-Castro, F., et al. Climate, irrigation, and land cover change explain streamflow trends in countries bordering the Northeast Atlantic. *Geophysical Research Letters* **2019**, *46*, 10821–10833. https://doi.org/10.1029/2019GL084084
134. Yousaf W, Awan WK, Kamran M et al. A paradigm of GIS andremote sensing for crop water deficit assessment in near realtime to improve irrigation distribution plan. *Agric Water Manag* **2021**, *243*, 106443. https://doi.org/10.1016/j.agwat.2020.106443
135. Vicente-Serrano, S. M., Zouber, A., Lasanta, T., & Pueyo, Y. Dryness is accelerating degradation of vulnerable shrublands in semiarid Mediterranean environments. *Ecological Monographs* **2012**, *82*(4), 407–428. https://doi.org/10.1890/11-2164.1
136. J.A. Sillero-Medina, J. González-Pérez, P. Hueso-González, J.J. González-Fernández, J.I. Hormaza-Urroz, J.D. Ruiz-Sinoga, Effect of different deficit irrigation regimens on soil moisture, production parameters of mango (Mangifera indica L.), and spectral vegetation indices in the Mediterranean region of Southern Spain. *Remote Sensing Applications: Society and Environment* **2025**, *37*, 101415. https://doi.org/10.1016/j.rsase.2024.101415

137. Sergio M. Vicente-Serrano, Ahmed El Kenawy, Dhais Peña-Angulo, Jorge Lorenzo-Lacruz, Conor Murphy, Jamie Hannaford, Simon Dadson, Kerstin Stahl, Iván Noguera, Magí Fraquesa, Beatriz Fernández-Duque, Fernando Domínguez-Castro, Forest expansion and irrigated agriculture reinforce low river flows in southern Europe during dry years. *Journal of Hydrology* **2025**, *653*, 132818. https://doi.org/10.1016/j.jhydrol.2025.132818
138. G. Moreno-Ortega, C. Pliego, D. Sarmiento, A. Barceló, E. Martínez-Ferri, Yield and fruit quality of avocado trees under different regimes of water supply in the subtropical coast of Spain. *Agricultural Water Management* **2019**, *221*, 192–201. https://doi.org/10.1016/j.agwat.2019.05.001
139. Romero Fresneda, R.; Moreno García, J.V.; Martínez Núñez, L.; Huarte Ituláin, M.T.; Rodríguez Ballesteros, C. and Botey Fullat, M.R. Comportamiento de las precipitaciones en España y periodos de sequía (periodo 1961-2018). Área de Climatología y Aplicaciones Operativas (AEMET) Ministerio para la Transición Ecológica y el Reto Demográfico, 2020. https://doi.org/10.31978/666-20-006-0.
140. Fonnegra Mora, Diana Carolina. Desarrollo de un sistema operativo para el cálculo de índices de sequía basados en información espacial. UNC digital repository, 2017. http://hdl.handle.net/11086/5991
141. Vicente-Serrano, S. M. Evaluating the impact of drought using remote sensing in a Mediterranean, semi-arid region. *Natural Hazards* **2007**, *40*, 173-208. https://doi.org/10.1007/s11069-006-0009-7
142. Vibhute, Amol & Kale, Karbhari & Dhumal, Rajesh & Mehrotra, Suresh. Soil type classification and mapping using hyperspectral remote sensing data. 2015 International Conference on Man and Machine Interfacing (MAMI) 1–4. https://doi.org/10.1109/MAMI.2015.7456607
143. Casella, A.; Barrionuevo, N.; Pezzola, A. and Winschel, C. Pre-processing of satellite images from the Sentinel 2a and 2b sensors using SNAP 6.0 software. Institute of Climate and Water. C.I.R.N. INTA Castelar, 2019. https://www.researchgate.net/publication/333091912_PRE-PROCESAMIENTO_DE_IMAGENES_SATELITALES_DEL_SENSOR_SENTINEL_2A_y_2B_CON_EL_SOFTWARE_SNAP_60/link/5cdafa15458515712eab6ea8/download?_tp=eyJjb250ZXh0Ijp7ImZpcnN0UGFnZSI6InB1YmxpY2F0aW9uIiwicGFnZSI6InB1YmxpY2F0aW9uIn19 (accessed on 24/03/2025).
144. Jordan, C.F. Derivation of Leaf Area Index from Quality of Light on the Forest Floor. *Ecology* **1999**, *50*, 663-666. http://dx.doi.org/10.2307/1936256
145. Welikhe, Pauline & Essamuah-Quansah, Joseph & Fall, Souleymane & McElhenney, Wendell. Estimation of Soil Moisture Percentage Using LANDSAT-based Moisture Stress Index. Journal of Remote Sensing & GIS. 06 2017. https://doi.org/10.4172/2469-4134.1000200
146. Arabzadeh, R., Kholoosi, M. M., & Bazrafshan, J. Regional hydrological drought monitoring using principal components analysis. *Journal of Irrigation and Drainage Engineering* **2016**, *142*(1), 04015029. Doi: 10.1061/(ASCE)IR.1943-4774.0000925
147. Haboudane, D., Miller, J.R., Pattey, E., Zarco-Tejada, P.J., Strachane, I.A. Hyperspectral vegetation indices and novel algorithms for predicting green LAI of crop canopies: Modeling and validation in the context of precision agriculture. *Remote Sensing of Environment* **2004**, *90*, 337–352. http://dx.doi.org/10.1016/j.rse.2003.12.013.
148. Schlemmer, M., Gitelsonb, A., Schepers, J., Fergusona, R., Peng, Y., Shanahana, J., Rundquist, R. Remote estimation of nitrogen and chlorophyll contents in maize at leaf and canopy levels. *International Journal of Applied Earth Observation and Geoinformation* **2013**, *25*, 47–54. https://doi.org/10.1016/j.jag.2013.04.003.
149. Marino, S.; Alvino, A. Vegetation Indices Data Clustering for Dynamic Monitoring and Classification of Wheat Yield Crop Traits. *Remote Sens.* **2021**, *13*, 541. https://doi.org/10.3390/rs13040541.

150. Longo-Minnolo, G., Consoli, S., Vanella, D., Guarrera, S., Manetto, G., & Cerruto, E. Delineating citrus management zones using spatial interpolation and UAV-based multispectral approaches. *Computers and Electronics in Agriculture* **2024**, *222*, 109098. https://doi.org/10.1016/j.compag.2024.109098.
151. Rinali Patel, Anant Patel. Evaluating the impact of climate change on drought risk in semi-arid regions using GIS technique. *Results in Engineering* **2024**, *21*, 101957. https://doi.org/10.1016/j.rineng.2024.101957.
152. Caliński, T., Harabasz, J. A dendrite method for cluster analysis. *Communications in Statistics* **1994**, *3*(1), 1–27. https://doi.org/10.1080/03610927408827101
153. Liu, Honghua & Yang, Jing & Ye, Ming & James, Scott & Tang, Zhonghua & Dong, Jie & Xing, Tongju. Using t-distributed Stochastic Neighbor Embedding (t-SNE) for cluster analysis and spatial zone delineation of groundwater geochemistry data. *Journal of Hydrology* **2021**, *597*, 126146. https://doi.org/10.1016/j.jhydrol.2021.126146
154. Verrelst, I., Camps-Valls. G., Muñoz-Marí, J., Rivera. J.P., Veroustraete, F., Clevers, J.G.P.W., Moreno, J. Optical remote sensing and the retrieval of terrestrial vegetation bio-geophysical properties – A review. *ISPRS Journal of Photogrammetry and Remote Sensing* **2015**, *108*, 273–290. https://doi.org/10.1016/j.isprsjprs.2015.05.005.
155. Vanegas F.; Bratanov, D.; Powell, K.; Weiss, J.; Gonzalez, F. A Novel Methodology for Improving Plant Pest Surveillance in Vineyards and Crops Using UAV-Based Hyperspectral and Spatial Data. *Sensors* **2018,** *18*(1), 260. https://doi.org/10.3390/s18010260.
156. Verrelst, J.; Rivera, J.P.; Veroustraete, F.; Muñoz-Marí, J.; Clevers, J.G.P.W.; Camps-Valls, G.; Moreno, J. Experimental Sentinel-2 LAI estimation using parametric, non-parametric and physical retrieval methods – A comparison. *ISPRS Journal of Photogrammetry and Remote Sensing* **2015**, *108*, 260–272. https://doi.org/10.1016/j.isprsjprs.2015.04.013.
157. Marković, M.; Goran, K.; Brkić, A.; Atilgan, A.; Japundžić-Palenkić, B.; Petrović, D.; Barač, Ž. Sustainable Management of Water Resources in Supplementary Irrigation Management. *Appl. Sci.* **2021**, *11*(6), 2451; https://doi.org/10.3390/app11062451.
158. Capstaff, N.M., Domoney, C. & Miller, A.J. Real-time monitoring of rhizosphere nitrate fluctuations under crops following defoliation. *Plant Method,* **2021**, *17*, 11. https://doi.org/10.1186/s13007-021-00713-w.
159. Clevers, J.G.P.W., Gitelsonb, A.A. Remote estimation of crop and grass chlorophyll and nitrogen content using red-edge bands on Sentinel-2 and -3. *International Journal of Applied Earth Observation and Geoinformation* **2013**, *23*, 344–351. https://doi.org/10.1016/j.jag.2012.10.008.
160. Rouse, J. W., Haas, R. H., Schell, J. A., Deering, D. W., & Harlan, J. C. Monitoring the vernal advancements and retrogradation of natural vegetation. In NASA/GSFC, Final Report, Greenbelt, MD, USA, 1973, pp. 1–137. https://www.semanticscholar.org/paper/Monitoring-the-Vernal-Advancement-and-(Green-Wave-Rouse-Haas/c3a30c40d304a7a312942c0c243f5033b8c3fd3f. (accessed on 29/03/2025).
161. Baret, F., Guyot, G. Potentials and limits of vegetation indices for LAI and APAR assessment. *Remote Sensing of Environment.* **1991**, *35*, 161–173. https://doi.org/10.1016/0034-4257(91)90009-U.
162. Solano, F., Di Fazio, S., Modica, G., A methodology based on GEOBIA and WorldView-3 imagery to derive vegetation indices at tree crown detail in olive orchards. *Int. J. Appl. Earth Obs. Geoinformation* **2019**, *83*, 101912. https://doi.org/10.1016/j.jag.2019.101912.
163. Pinto, J., Rueda-Chacón, H., Arguello, H., Pinto, J., Rueda-Chacón, H., Arguello, H., Classification of Hass avocado (persea americana mill) in terms of its ripening via hyperspectral images. *Tecnológicas* **2019**, *22*, 111–130. https://doi.org/10.22430/22565337.1232.

 doi:10.20944/preprints202509.1149.v1

164. Cui, B.; Zhao, Q.; Huang, W.; Song, X.; Ye, H.; Zhou, X. A New Integrated Vegetation Index for the Estimation of Winter Wheat Leaf Chlorophyll Content. *Remote Sens.* **2019**, *11*, 974. https://doi.org/10.3390/rs11080974.
165. Kira, O.; Linker, R.; Gitelson, A. No destructive estimation of foliar chlorophyll and carotenoid contents Focus on informative spectral bands. *International Journal of Applied Earth Observation and Geoinformation* **2015**, *38*, 251–260. http://dx.doi.org/10.1016/j.jag.2015.01.0030303-2434. Available from: https://www.researchgate.net/publication/281818833_Non_destructive_estimation_of_foliar_chlorophyll_and_carotenoid_contents_Focus_on_informative_spectral_bands (accessed on 26/05/2021).
166. Gallardo, J.L. and Pompa, M. Detecting Individual Tree Attributes and Multispectral Indices Using Unmanned Aerial Vehicles: Applications in a Pine Clonal Orchard. *Remote Sens*. **2020**, *12*, 4144; https://doi.org/10.3390/rs12244144.
167. Hardy, C.C. and Burgan, R.E. Evaluation of NDVI for monitoring live moisture in three vegetation types of the Western U.S. *Photogrammetric Engineering & Remote Sensing* **1999**, *65* (5), 603-610. Available online: https://www.asprs.org/wp-content/uploads/pers/1999journal/may/1999_may_603-610.pdf. (accessed on 20/05/2025).
168. Chuvieco, E; Riaño, D.; Aguado, I.; Cocero, D. Estimation offuel moisture content from multitemporal analysis of Landsat Thematic Mapper reflectancedata: Applications in fire danger assessment, International *Journal of Remote Sensing* **2002**, *23* (11), 2145–2162. https://doi.org/10.1080/01431160110069818.
169. Dennison, P.E. Corresponding author, Roberts, D. A.; Peterson, S. H.; Rechel, J. Use of Normalized Difference Water Index for monitoring live fuel moisture. *International Journal of Remote Sensing* **2005**, *26* (5), 1035–1042. https://doi.org/10.1080/0143116042000273998.
170. Ren, H. and Zhoub, G. Estimating green biomass ratio with remote sensing in arid grasslands. *Ecological Indicators* **2019**, *98*, 568-574. https://doi.org/10.1016/j.ecolind.2018.11.043.
171. Ullah, S.; Si, Y.; Schlerf, M.; Skidmore, A.K.; Shafique, M.; Iqbal, I.A. Estimation of grassland biomass and nitrogen using MERIS data. *International Journal of Applied Earth Observation and 172Geoinformation*, **2012**, *19*, 196–204. https://doi.org/10.1016/j.jag.2012.05.008.
172. Peñuelas, J.; Baret, F.; Filella; I. Semi-empirical indices to assess carotenoids/chlorophyll a ratio from leaf spectral reflectance. *Photosynthetica* **1995**, *31*(2), 221–230. https://d1wqtxts1xzle7.cloudfront.net/40129540/Semi-empirical_indices_to_assess_caroten20151118-6483-4696yg-with-cover-page.pdf?Expires=1622112454&Signature=GbGZra6VblWwdL17Lq03aE1f~Jxt7os75o4depfh1gYJEhyp6kM9sI~9w8yHvddNwC7XLxsG8DkbUDbRGvwu5i0vfwxZLWya-77RsnJuA4Gk2mTe~ss5FEHU3TORqmlstlSaXvLLCAMbAOAnLpYk5SRClVgV5VUScqXkl2xNuCCuMCBv618mD75Db054SMGzfGGX1OHBIvYw~wV7pBaBQtJrNxnrrR6SsZoGiHLHWr2QeJc6zX1dLcXTVShfBZdYxe1EYmdpw~D5oVWu4FiN0OprbZ-9ISEyj2xFbCnyst-V1GXVAay7UgWvRlkkPpGZztfhKm-0aCnWqrxyxEsfA__&Key-Pair-Id=APKAJLOHF5GGSLRBV4ZA. (accessed on 23/05/2025).
173. Baret, F.; Clevers, J.G.P.W.; Steven, M.D. The robustness of canopy gap fraction estimates from red and near-infrared reflectances: A comparison of approaches. *Remote Sensing of Environment* **1995**, *54* (2), 141–151. https://doi.org/10.1016/0034-4257(95)00136-O.
174. Gitelson, A.A.; Peng, Y.; Arkebauer, T.J.; Schepers, J. Relationships between gross primary production, green LAI, and canopy chlorophyll content in maize: Implications for remote sensing of primary production. *Remote Sensing of Environment* **2014**, *144*, 65-72. https://doi.org/10.1016/j.rse.2014.01.004.

175. Yang, F.; Sun, J.; Fang, H.; Yao, Z.; Zhang, J.; Zhu, Y.; Song, K.; Wang, Z.; Hu, M. Comparison of different methods for corn LAI estimation over northeastern China. *International Journal of Applied Earth Observation and Geoinformation* **2012**, *18*, 462–471. https://doi.org/10.1016/j.jag.2011.09.004.
176. Nguy-Robertson, A.L.; Peng, Y.; Gitelson, A.A.; Arkebauer, T.J.; Pimstein, A.; Herrmann, I.; Karnieli, A.; Rundquist, D.C.; Bonfil, D.J. Estimating green LAI in four crops: Potential of determining optimal spectral bands for a universal algorithm. *Agricultural and Forest Meteorology* **2014**, *192–193*, 140–148. https://doi.org/10.1016/j.agrformet.2014.03.004.
177. Darvishzadeh, R.; Atzberger, C.; Skidmore, A.; Schlerf, M. Mapping grassland leaf area index with airborne hyperspectral imagery: A comparison study of statistical approaches and inversion of radiative transfer models. *ISPRS Journal of Photogrammetry and Remote Sensing* **2011**, *66* (6), 894–906. https://doi.org/10.1016/j.isprsjprs.2011.09.013.
178. Feng, W., Wu, Y., He, L. *et al.* An optimized non-linear vegetation index for estimating leaf area index in winter wheat. *Precision Agric.* **2019**, *20*, 1157–1176. https://doi.org/10.1007/s11119-019-09648-8.
179. Ramírez-Gil, J.G., Henao-Rojas, J.C., Morales-Osorio, J.G. Postharvest diseases and disorders in avocado cv. Hass and their relationship to preharvest management practices. *Heliyon* **2021**, *7*, 05905. https://doi.org/10.1016/j.heliyon.2021.e05905.
180. Granero-Belinchón, C.; Adeline; K.; Lemonsu, A.; Briottet, X. Phenological Dynamics Characterization of Alignment Trees with Sentinel-2 Imagery: A Vegetation Indices Time Series Reconstruction Methodology Adapted to Urban Areas. *Remote Sens.* **2020**, *12*(4), 639. https://doi.org/10.3390/rs12040639.
181. Di Bella, C.M.; Paruelo, J.M.; Becerra, J.E.; Bacour, C.; Baret, F. Effect of senescent leaves on NDVI-based estimates of APAR: Experimental and modelling evidence. *International Journal of Remote Sensing*, **2004**, *25* (23), 5415–5427, https://doi.org/10.1080/01431160412331269724.
182. Zhang, Y.; Xiao, X.; Jin, C.; Dong, J.; Zhou, Z.; Wagle, P.; Joiner, J.; Guanter, L.; Zhang, Y.; Zhang, G.; Qin, Y.; Wang, J.; Moore III, B. Consistency between sun-induced chlorophyll fluorescence and gross primary production of vegetation in North America. *Remote Sensing of Environment* **2016**, *183*, 154–169. https://doi.org/10.1016/j.rse.2016.05.015
183. He, M.; Ju, W.; Zhou, Y.; Chen, J.; He, H.; Wang, Sh.; Wang, H.; Guan, D.; Yan, Y.; Li, Y.; Hao, Y.; Zhao, F. Development of a two-leaf light use efficiency model for improving the calculation of terrestrial gross primary productivity. *Agricultural and Forest Meteorology* **2013**, *173*, 28–39. http://dx.doi.org/10.1016/j.agrformet.2013.01.003.
184. Piao, Sh.; Mohammat, A.; Fang, J.; Cai, Q.; Feng, J. NDVI-based increase in growth of temperate grasslands and its responses to climate changes in China. *Global Environmental Change* **2006**, *16*(4), 340–348. https://doi.org/10.1016/j.gloenvcha.2006.02.002.
185. Bastin, G.; Scarth, P.; Chewings, V.; Sparrow, A.; Denham, R.; Schmidt, M.; O'Reagain, P.; Shepherd, R.: Abbott, B. Separating grazing and rainfall effects at regional scale using remote sensing imagery: A dynamic reference-cover method. *Remote Sensing of Environment* **2012**, *121*, 443–457. https://doi.org/10.1016/j.rse.2012.02.021.